

The Properties of Sub-mm Galaxies in Hierarchical Models

A. M. Swinbank^{1,*}, C. G. Lacey¹, Ian Smail¹, C. M. Baugh¹, C. S. Frenk¹,
 A. W. Blain², S. C. Chapman³, K. E. K. Coppin¹, R. J. Ivison^{4,5}, L. J. Hainline⁶,
 J. E. Gonzalez¹

¹*Institute for Computational Cosmology, Department of Physics, Durham University, South Road, Durham, DH1 3LE, UK*

²*Astronomy Department, California Institute of Technology, 105-24, Pasadena, CA 91125, USA*

³*Institute of Astronomy, University of Cambridge, Madingley Road, Cambridge, CB3 0HA, UK*

⁴*UK Astronomy Technology Center, Royal Observatory, Blackford Hill, Edinburgh, EH19 3HJ, UK*

⁵*Institute for Astronomy, University of Edinburgh, Edinburgh, EH19 3HJ, UK*

⁶*Department of Astronomy, University of Maryland, College Park, MD 20742, USA*

**Email: a.m.swinbank@durham.ac.uk*

31 October 2021

ABSTRACT

We use the combined GALFORM semi-analytical model of galaxy formation and GRASIL spectrophotometric code to investigate the properties of galaxies selected via their sub-millimeter (sub-mm) emission. The fiducial model we use has previously been shown to fit the properties of local ULIRGs, as well as the number counts of faint sub-mm galaxies. Here we test the model in more detail by comparing the SEDs and stellar, dynamical, gas and halo masses of sub-mm galaxies against observational data. We precisely mimic the sub-mm and radio selection function of the observations and show that the predicted far-infrared properties of model galaxies with $S_{850} > 5$ mJy and $S_{1.4} > 30\mu\text{Jy}$ are in good agreement with observations. Although the dust emission model does not assume a single dust temperature, the far-infrared SEDs are well described by single component modified black-body spectrum with characteristic temperature 32 ± 5 K, in good agreement with observations. We also find evidence that the observations may have uncovered evolution in the far-infrared–radio relation in ULIRGs out to $z \sim 2$. We show that the predicted redshift distribution of sub-mm galaxies provides a reasonable fit to the observational data with a median redshift $z = 2.0$. The radio-selected subset of sub-mm galaxies are predicted to make up approximately 75% of the population and peak at $z = 1.7$, in reasonable agreement with the observed radio detected fraction and redshift distribution. However, the predicted K -band and mid-infrared ($3\text{--}8\mu\text{m}$) flux densities of the sub-mm galaxies (and LBGs) are up to a factor $10\times$ fainter than observed. We show that including the stellar TP-AGB phase in the stellar population models does not make up for this deficit. This discrepancy may indicate that the stellar masses of the sub-mm galaxies in the model are too low: $M_{\star} \sim 10^{10} M_{\odot}$, while observations suggest more massive systems, $M_{\star} \gtrsim 10^{11} M_{\odot}$. However, if the predicted K - and $3\text{--}8\mu\text{m}$ extinctions in the model could be dramatically reduced, then this would reduce, but not eliminate, this discrepancy. Finally we discuss the potential modifications to the models which may improve the fit to the observational data, as well as the new observational tests which will be made possible with the arrival of new facilities, such as SCUBA2.

Key words: galaxies: evolution – galaxies: formation – galaxies: high-redshift – sub-millimeter

1 INTRODUCTION

The discovery a decade ago of a population of faint submm-selected galaxies (SMGs) revolutionised our view of the cosmic star formation history of the Universe (Smail et al. 1997;

Hughes et al. 1998; Barger et al. 1998). These galaxies (originally discovered with the SCUBA instrument at $850\mu\text{m}$) appear to be high redshift galaxies with star-formation rates exceeding $1000M_{\odot}\text{yr}^{-1}$ (Ivison et al. 2000; Smail et al. 2002). These Ultra-Luminous Infrared Galaxies (ULIRGs)

peak around $z \sim 2$ (Chapman et al. 2003, 2005) and show a thousand fold increase in their abundance between $z = 0$ and $z = 2$. If this far-infrared emission arises solely from star-formation with a standard (“solar neighborhood”) IMF, then they could potentially dominate the star-formation activity in the early Universe, dwarfing the contribution of galaxies selected in the rest-frame ultraviolet. The apparent intensity of these starbursts, the resulting high metallicity, along with their large dynamical masses, high gas fractions and inferred strong clustering (Blain et al. 2004b; Greve et al. 2005; Tacconi et al. 2006, 2008; Swinbank et al. 2004, 2006) are all suggestive of a close link to the formation phase of the most massive spheroids and black holes (Lilly et al. 1999; Smail et al. 2002, 2004; Webb et al. 2003; Genzel et al. 2003; Smail et al. 2004; Alexander et al. 2003, 2005; Swinbank et al. 2006).

Reproducing the sub-mm galaxy population has been a major challenge for theoretical models (Granato et al. 2000; Baugh et al. 2005). In part this is because (quite reasonably) many of the recipes and constraints used to develop the models are based on the formation and evolution of “normal” galaxies rather than the extreme populations. Hence these models have had difficulty reproducing extremely luminous galaxies with sufficient cool dust at high redshift without over-predicting the abundance of bright galaxies in the local Universe. Initial attempts to match the basic properties of sub-mm galaxies (whilst maintaining the match to the present day K -band luminosity function and $IRAS\ 60\mu\text{m}$ luminosity function) under-predicted the $850\mu\text{m}$ counts by a factor $30\times$ (Baugh et al. 2005) despite ΛCDM producing enough baryons in massive halos at $z \sim 2$ to match observations of gas masses in sub-mm galaxies (Genzel et al. 2003; Greve et al. 2005).

One solution to this problem was to alter the Initial Mass Function (IMF): Blain et al. (1999) suggested that a Salpeter IMF (Salpeter 1955) with a low-mass threshold of $3M_{\odot}$ was required in far-infrared luminous galaxies around $z \sim 2$ since the implied star-formation rate for a Salpeter IMF integrated to the canonical value of $0.07M_{\odot}$ would over-predict the integrated stellar density at $z = 0$. Invoking a top-heavy (or “flat”) IMF in the semi-analytic framework has been shown to provide a much improved fit to the sub-mm galaxy counts and redshift distribution as well as the Lyman-break galaxy luminosity function whilst still maintaining a good fit to the properties of the present day galaxy populations (Baugh et al. 2005, hereafter B05). In this model, a standard IMF is adopted in quiescently star-forming galaxies, whilst the star-formation induced by galaxy mergers produces stars with a flat IMF: $dn/d\ln(m) = m^{-x}$ with $x = 0$ (compared to a Salpeter IMF which has $x = 1.35$; Salpeter 1955). With a larger proportion of high mass stars, the energy radiated in the ultra-violet per unit mass of stars produced is increased, thus increasing the amount of radiation to heat the dust. Moreover, the flat IMF produces a higher yield of metals from type II supernovae, thus increasing the dust content of the galaxy and boosting the luminosity in the sub-millimeter waveband.

This assumption of a flat IMF in bursts is controversial and so it is essential to explore the predictions of this model in more detail. In particular, the model can be (i) tested against the growing observational multi-wavelength data on sub-mm galaxies to test whether the choice of parameters is

suitable and (ii) provide useful constraints on observational data, in particular for understanding possible selection biases. For example, since much of what is known about sub-mm galaxies is based on the radio-detected sub-sample, one outstanding issue is how much this radio-selection (which does not benefit from the negative K-correction experienced in the sub-mm waveband) has affected the conclusions being drawn about SMGs. Are the radio-undetected fraction of SMGs at either significantly higher redshift (Younger et al. 2007) or do they instead have far-infrared colours which represent much colder systems (Chapman et al. 2005)?

In §2 we describe the basic properties of the galaxy formation model we employ, but refer the reader to Cole et al. (2000), Benson et al. (2002, 2003), Baugh et al. (2005) and Lacey et al. (2008) for a detailed description. In §3 we test the predicted far-infrared properties of sub-mm-selected galaxies against the available observational data. In §4 we discuss the masses and evolution of model SMGs compared to those estimated from observational data and in §5 we give our conclusions and future prospects for constraining the properties of sub-mm galaxies both theoretically and observationally. We use a flat, ΛCDM cosmology with $\Omega_m = 0.3$, $\sigma_8 = 0.93$ and $H_o = 100h \text{ km s}^{-1} \text{ Mpc}^{-1}$ with $h = 0.7$.

2 THE MODEL

The galaxy formation model which we employ is the one described in detail in Baugh et al. (2005) and Lacey et al. (2008). The model is based on the semi-analytic code of Cole et al. (2000) with important revisions described in Benson et al. (2002, 2003) and is reviewed extensively in Baugh (2006). In summary, the formation, assembly and evolution of galaxies are calculated using a background cosmology in which the dark matter structure grows hierarchically. The physical ingredients considered in the model include: (i) The formation of dark matter halos through mergers and accretion of material. (ii) The collapse of baryons into the gravitational potential wells of dark matter halos. (iii) The radiative cooling of gas that is shock heated during infall into the dark halo. (iv) The formation of a rotationally supported disk of cold gas. (v) The formation of stars from the cold gas. (vi) The injection of energy into the interstellar medium, through supernova explosions or the accretion of material onto a super-massive black hole. (vii) The chemical evolution of the interstellar medium, stars and the hot gas. (viii) The merger of galaxies following the merger of their host dark matter halos, due to dynamical friction. (ix) The formation of spheroids during mergers due to the rearrangement of pre-existing stars (i.e. the disk and bulge of the progenitor galaxies) and the formation of stars in a burst. (x) The construction of a star-formation history and a composite stellar population for each galaxy.

The spectral energy distribution (SED) from this composite stellar population is calculated using the spectrophotometric model GRASIL (Silva et al. 1998). GRASIL computes the emission from both the stars and dust in a galaxy, based on the star formation, metal enrichment history and the sizes as predicted by the semi-analytical model (Granato et al. 2000). GRASIL includes radiative transfer through a two-phase dust medium, with a diffuse component and giant molecular clouds, and a distribution of dust grain sizes. We

note that GRASIL does not assume a single dust temperature for the galaxy. Stars are assumed to form inside the clouds and then gradually migrate out. The output from GRASIL is the galaxy SED from the far-UV to radio wavelengths.

2.1 Radio Emission and the Far-Infrared–Radio Correlation

In addition to the sub-mm/far-infrared emission from dust, the radio emission is also included in the model following Bressan et al. (2002). The radio emission is produced by (i) thermal bremsstrahlung from HII regions and (ii) synchrotron radiation powered by acceleration of relativistic electrons in supernova remnants. In local galaxies, there is a strong correlation between non-thermal radio and far-infrared emission, holding over five decades of luminosity (e.g. Helou et al. 1985; Yun et al. 2001; Vlahakis et al. 2007). The standard explanation of this relationship is that both the far-infrared and the bulk of the radio emission are caused by high-mass ($\gtrsim 5 M_{\odot}$) stars. These stars both heat the dust (which then emits far-infrared emission) and at the end of their lives explode as supernovae (see e.g. Condon 1992 and references therein), producing the relativistic electrons responsible for synchrotron radiation. The strength of this synchrotron emission depends on not only the number density of relativistic electrons, but also the strength of the magnetic field. The rate of energy input into the relativistic electrons depends on the assumed low-mass cut off for Type II supernova production, which is usually taken as $8 M_{\odot}$ (Bressan et al. 2002).

In the model galaxies, both the thermal and non-thermal contributions to the radio emission are calculated. The thermal component of the radio emission is estimated from the stellar emission essentially without free parameters, assuming that all ionizing photons are absorbed by gas within the galaxy, and is proportional to the instantaneous ionizing luminosity of the stars. The synchrotron (non-thermal) radio emission is assumed to be proportional to the instantaneous Type II supernova rate, but its calculation involves two empirical parameters, which are essentially the efficiency with which the supernova explosion energy is converted into energy of relativistic electrons, and the power-law index of the injection energy spectrum of these relativistic electrons, which determines the spectral index of the synchrotron emission. It is assumed that the radiative lifetime of the relativistic electrons is short enough that the total synchrotron luminosity is always equal to the instantaneous energy injection rate from supernovae. Bressan et al. (2002) estimate both of these parameters from observations of local galaxies; in particular, the efficiency factor was chosen based on observations of the Milky Way galaxy. They found that this choice also reproduced the observed ratio of radio to far-infrared emission for normal spirals. In this model, the ratios between the far-infrared and radio luminosities and the instantaneous star formation rate (SFR) all approach constant values if the SFR varies only on timescales $\gtrsim 100$ Myr (as in normal spirals). However, due to the different lifetimes of the stars powering the far-infrared, thermal and non-thermal radio emission, there are timelags between the corresponding luminosities and the formation of the stars involved, and so these ratios vary if the SFR changes on timescales $\lesssim 100$ Myr, as is the case in starbursts.

This is discussed in detail in Bressan et al. (2002), and has consequences for the results in this paper.

In Fig. 1 we show the far-infrared–radio ($60\mu\text{m}$ versus 1.4 GHz) correlation for local star-forming galaxies and overlay the model predictions for galaxies at $z < 0.1$. This shows that the model reproduces the form of the observed far-infrared–radio correlation at lower luminosities. However, at higher luminosities the predicted radio–far-infrared relation lies below that observed (Helou et al. 1985; Yun et al. 2001; Vlahakis et al. 2007), by a factor $3.2 \pm 0.2\times$, assuming the Bressan et al. (2002) normalisation of the radio emission using the Milky Way. As we are interested in the evolution of SMGs, which have ULIRG-like luminosities ($L_{\text{bol}} > 10^{12} L_{\odot}$) and appear likewise to be dusty starbursts, it seems appropriate to renormalize the non-thermal radio emission in the model so that it matches the properties of high-luminosity *IRAS*-selected samples at $z = 0$. This seems likely to produce the most realistic estimates for the radio luminosities of SMGs, in the framework of the present galaxy formation model. Physically, this renormalization corresponds to assuming a higher efficiency for conversion of supernova blastwave energy into energy of relativistic electrons in starbursts as compared to normal spirals, which might result from the higher densities or magnetic fields in starbursts. In the present paper, we have therefore multiplied the non-thermal radio luminosities from GRASIL by a factor 3.2, as shown in Fig. 1. We note that this renormalization might not be needed at $z = 0$ in a galaxy formation model which predicts significantly different burst timescales in ULIRGs. Indeed, Bressan et al. (2002) reproduced the SED of the ULIRG Arp220, including its radio emission, using their standard synchrotron normalization, but treating the burst timescale as a free parameter. However, in our galaxy formation model, the burst timescales are already fixed by other considerations.

In what follows, we parameterize the relative strength of the far-infrared and radio emission using q_L , defined as $q_L = \log(L_{\text{bol}} / ([4.52 \text{ THz}] L_{1.4 \text{ GHz}}))$ where L_{bol} is the total dust luminosity and $L_{1.4 \text{ GHz}}$ is the rest-frame radio luminosity. The latter is calculated from the observed 1.4GHz flux $S_{1.4}$ using $L_{1.4 \text{ GHz}} = 4\pi D_L^2 S_{1.4} (1+z)^{\alpha-1}$, where the spectral index, α , has a typical value of 0.7 for non-thermal sources; Condon 1992). For local ULIRGs, q_L is measured to be $q_L = 2.34 \pm 0.01$ with $\sigma_{q_L} = 0.10$ (e.g. Yun et al. 2001). As described above, we have normalised the radio emission of $z < 0.1$ model ULIRGs so that by construction they have $q_L = 2.34$. The model predicts a dispersion $\sigma_{q_L} = 0.11$. We stress that this renormalisation ensures that our model agrees with observations of the radio and far-infrared emission of galaxies in the luminosity range appropriate for SMGs in the local Universe. However, the model also predicts evolution in these quantities. For an exponentially declining star-formation rate with a top-heavy IMF, the radio flux density will plateau shortly after the initial burst since the SNe are produced from stars with mass $\gtrsim 8 M_{\odot}$ which have lifetimes of approximately 50 Myrs. In contrast, the far-infrared luminosity will continue to increase for longer as dust is produced and then heated by new generations of stars extending down to lower masses $\gtrsim 5 M_{\odot}$. As a result, the value of q_L is not constant for bursts, but depends both on the SFR timescale and on the age at which the burst is observed (Bressan et al. 2002).

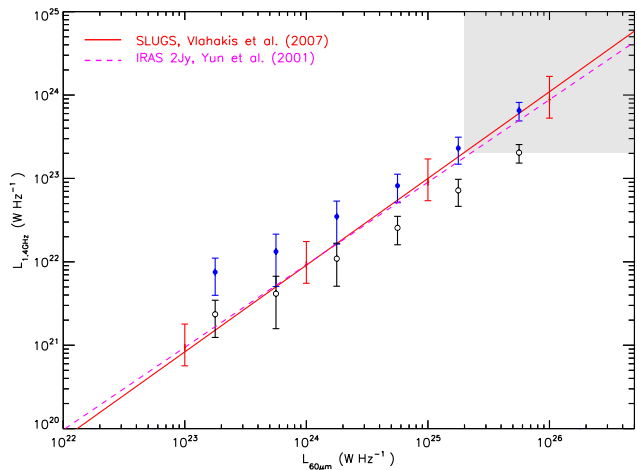


Figure 1. Far-Infrared – radio correlation for galaxies in the GRASIL model compared to the SCUBA Local Galaxy Survey (SLUGS) and IRAS 2Jy survey from Yun et al. (2001) and Vlahakis et al. (2007). The red error-bars show the scatter in the observed data. The shaded area denotes the approximate $60\mu\text{m}$ and radio luminosities encompassing the ULIRGs from Sanders et al. (2003). The model ($z < 0.1$) predictions are overlaid for both the original radio luminosities (open circles) and after the renormalisation factor $3.2\times$ has been applied to the radio flux densities (filled circles). We adopt this renormalisation of the model to ensure that it reproduces the far-infrared and radio properties of local galaxies with luminosities comparable to those observed for high-redshift SMGs – giving us a reliable local benchmark.

The average q_L in bursts therefore depends both on redshift and on how the galaxy sample is selected. For model ULIRGs at $z = 2$ (which overlap substantially with SMGs), we find $q_L = 2.19 \pm 0.05$ and $\sigma_{q_L} = 0.26$. Moreover, the e-folding timescale for star formation in model ULIRGs more than halves between $z = 0$ and $z = 2$ ($\tau_{eff} = 300_{-150}^{+250}$ Myr at $z = 0$ compared to 130_{-60}^{+150} Myr at $z = 2$). In addition, the median age of the burst in model ULIRGs at $z = 2$ is much shorter than at $z = 0$ (8_{-6}^{+50} compared to 50_{-40}^{+400} Myr). The young ages of the high-redshift model ULIRGs, combined with the time-lag between the onset of the burst and the production of the first supernova, thus results in an evolution in the far-infrared–radio relation for these luminous galaxies. We will return to this point when studying the radio and far-infrared properties of SMGs later.

3 ANALYSIS

3.1 Simulating Sub-mm Catalogues

To test the GALFORM/GRASIL model we need to compare its predictions to the detailed multi-wavelength properties of high-redshift sub-mm galaxies. To achieve this we have to focus on samples with reliable galaxy identification (which has so far relied on high resolution radio imaging), and follow-up spectroscopy to provide precise and unambiguous redshifts. By far the largest and most secure redshift survey of sub-mm galaxies comes from (Chapman et al. 2005 hereafter C05) who surveyed a total area of approximately 0.25 degree² across seven fields, securing spectroscopic redshifts

for 73 sub-mm galaxies with $850\mu\text{m}$ flux densities $\geq 5\mu\text{Jy}$ and radio counterparts with flux densities $S_{1.4} \geq 30\mu\text{Jy}$. This comprises the primary comparison sample for our analysis.

The C05 survey relies on radio identification as the only secure method to pin-point the counterparts of large samples of the sub-mm emitting galaxies. This is because the large beam-size ($\sim 15''$ for the JCMT at $850\mu\text{m}$) conspires with the large number of possible counterparts making it impossible to identify the galaxy responsible for the far-infrared emission with $850\mu\text{m}$ imaging alone; (Smail et al. 2000; Ivison et al. 1998, 2000, 2002, 2005, 2007). Using the deepest radio imaging currently available ($\sigma \sim 5\text{--}10\mu\text{Jy}$), this radio selection identifies $\sim 65\text{--}80\%$ of the bright ($S_{850} > 5\text{mJy}$) sub-mm galaxies (Ivison et al. 2005, 2007), but potentially introduces biases when extrapolating the properties of radio identified sub-mm galaxies to the whole population. We investigate the effect of this bias in the model by defining two classes of sub-mm galaxy: first, all sub-mm galaxies with $S_{850} > 5\text{mJy}$ are called SMGs; second, we define the subset of this population which are detectable in the radio (with $S_{850} > 5\text{mJy}$ and $S_{1.4} > 30\mu\text{Jy}$) as radio-identified sub-mm galaxies or rSMGs.

In order to simulate observational sub-mm catalogues, we must model the measurement noise. In particular, since most sub-mm catalogues are cut at a threshold around $3.5\text{--}4\sigma$, sub-mm maps suffer from *flux boosting* in which the flux limit of low significance sources can be increased above the survey signal-to-noise due to (a) confusion (the contribution of fainter sources within the large beams) and (b) the inclusion of low-significance sources which are boosted above the survey signal-to-noise due to the coincidence alignment with positive noise spikes. In order to properly compare the observations with the models we therefore convolve the model sub-mm and radio flux densities with a typical $1\text{-}\sigma$ noise of $\sigma_{850} = 1.5\text{mJy}$ (e.g. Scott et al. 2002; Coppin et al. 2007) and $\sigma_{1.4} = 5\text{--}10\mu\text{Jy}$ respectively (e.g. Ivison et al. 2002, 2007), thus allowing a like-for-like comparison with observations. This measurement noise is assumed in all following sections and analysis, and is included in all of the estimates which we give for average masses and luminosities of model galaxies.

3.2 Number Counts, Redshift Distribution and Space Density of SMGs

In Fig. 2 we show the predicted cumulative source counts as a function of $850\mu\text{m}$ flux density compared to the observations derived from a number of different surveys with SCUBA. The fiducial model of B05 agrees well with the observations down to the deepest flux density limits, with the model counts above 0.1mJy being dominated by ongoing merger-driven bursts at high-redshift, as these authors demonstrated.

To determine the effect of the radio-preselection on the number counts, we also show the cumulative source counts for galaxies which also have radio flux densities $S_{1.4} > 30\mu\text{Jy}$. At a characteristic $850\mu\text{m}$ flux density limit of 5mJy of C05, the model suggests that the radio detected fraction is $\sim 75\%$, consistent with the fraction typically found in sub-mm surveys ($65\text{--}80\%$) (Ivison et al. 2005, 2007).

The redshift distribution of the radio-identified SMGs

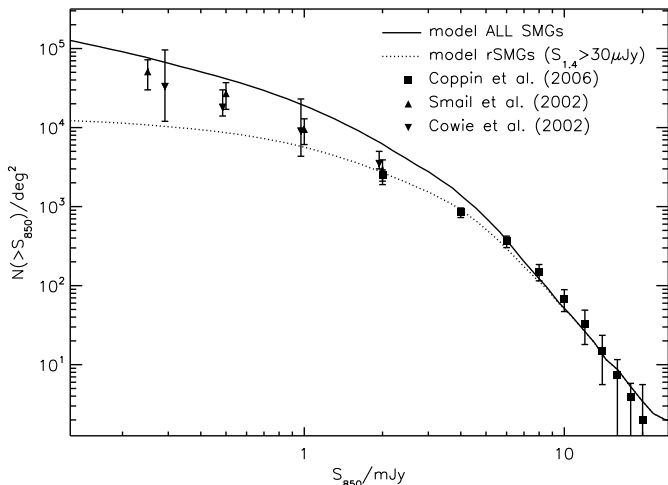


Figure 2. The cumulative number counts per degree² at 850 μ m as a function of sub-mm flux density. The model predictions are shown for SMGs and rSMGs respectively. We also plot the observational results from various surveys with SCUBA on the JCMT (Smail et al. 2002; Cowie et al. 2002; Coppin et al. 2006). Above 5 mJy, the model suggests that the surface density of sub-mm galaxies with radio flux densities above 30 μ Jy is 75%. This agrees well with the observed radio-detected fraction of $S_{850} > 5$ mJy, $S_{1.4} > 30\mu$ Jy sub-mm galaxies of 65-80% (Ivison et al. 2005, 2007).

from C05 (crudely corrected for spectroscopic incompleteness due to the redshift desert) is well fit by a Gaussian profile with a median redshift $z = 2.0$ and $\sigma_z = 0.7$. Using a simple model to account for radio incompleteness, C05 estimate the underlying redshift distribution of SMGs to peak at $z = 2.2$ with a 1- σ width of $\sigma_z = 1.3$.

In Fig. 3 we show the redshift distribution of SMGs and rSMGs in the fiducial model of B05 compared to observations. The model SMGs have a median redshift of $\langle z \rangle = 2.0$ with $\sigma_z = 1.0$. However, as Fig. 3 also shows, the radio-identified sub-set peaks at $\langle z \rangle = 1.7$ with $\sigma_z = 0.8$. Although there is reasonable overlap between the model and observations, the model SMGs and rSMGs both appear to peak at slightly lower redshift than inferred observationally ($\Delta z \sim 0.2-0.3$ in both cases). We note that the field-to-field variation between the seven sub-fields in the C05 sample is $\Delta z \sim 0.25$. This may be a simple reflection of the fact that SMGs are highly clustered (Blain et al. 2004b), and so we expect that the redshift distribution from C05 is likely to be uncertain by at least this amount due to cosmic variance. Therefore we conclude that the model and observations are in good agreement.

It is also worth noting that Clements et al. (2008) derive a median redshift $z \sim 1.5$ using photometric redshifts (rising to $z \sim 1.9$ when including the far-infrared photometry) for a similar sample of radio and mid-infrared identified SMGs from the SHADES submm survey. However, as Clements et al. (2008) note, there are large errors on photometric redshifts for sub-mm galaxies ($\Delta z \sim 0.5-1$), especially for the sources with the faintest counterparts. Nevertheless, their results are also consistent with the model redshift distributions for the rSMGs.

Using the number counts and redshift distribution, we

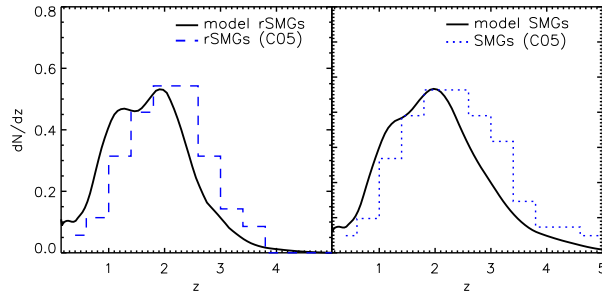


Figure 3. The predicted redshift distribution of model SMGs and rSMGs. *Left:* $N(z)$ for galaxies selected at both sub-mm and radio- wavelengths. The median redshift in the model rSMGs is $z = 1.7$ with $\sigma_z = 0.8$. We over-plot the redshift distribution of rSMGs from Chapman et al. (2005) (corrected for spectroscopic incompleteness in the redshift desert). *Right:* $N(z)$ for a pure sub-mm selected sample of galaxies with 850 μ m flux densities greater than 5 mJy, peaking at $z = 2.0$ with $\sigma_z = 1.0$. Again we over-plot the redshift distribution from Chapman et al. (2005), corrected for spectroscopic incompleteness and radio incompleteness using a simple model for the evolution of the radio luminosity function. In both panels, the redshift distribution for the model galaxies is slightly shallower than the observations suggest (by $\Delta z \sim 0.2-0.3$), although since the field-to-field variance in the observations is $\Delta z \sim 0.25$ we conclude that (within the observational uncertainties) the redshift distributions are in good agreement.

can also compare the space densities. The observed space density of rSMGs from C05 indicates that between $z = 0.9-3.5$ the volume density should be $\sim 8.0 \times 10^{-6} \text{ Mpc}^{-3}$. In comparison, the predicted space density for model rSMGs in the same redshift interval is $1.1 \pm 0.1 \times 10^{-5} \text{ Mpc}^{-3}$, slightly higher but consistent with the observations. In Fig. 4 we show the space densities over the redshift interval $z = 0.9-3.5$ for the model SMGs compared to the SMGs in the C05 sample. To interpret this data as a cumulative luminosity function, we also convert the number counts and 850 μ m flux densities to approximate space densities and bolometric luminosities assuming a median redshift $z = 2.0$.

3.3 Far-infrared Spectral Properties

Constraining the far-infrared SED of sub-mm galaxies is a key observational goal since the thermal emission from cold dust dominates the bolometric luminosity of these galaxies ($L_{8-1000\mu\text{m}} \gtrsim 0.95 L_{\text{bol}}$). Sub-mm photometry (at wavelengths other than 850 μ m) can be used to constrain the SED, measuring the apparent temperature of the dust, and infer their far-infrared luminosity and thus star-formation rate (assuming an IMF). These diagnostics also allow these galaxies to be placed in the context of other populations of high-redshift star-forming galaxies and active galactic nuclei (AGN).

To test how well the SEDs predicted by the model galaxies reproduce the dust emission spectra of SMGs, we compare the predicted far-infrared colours with existing observational data.

3.3.1 1200/850 μ m Colours

First, we compare the 850 μ m flux density ratio with longer wavelength photometry. In particular, it has been

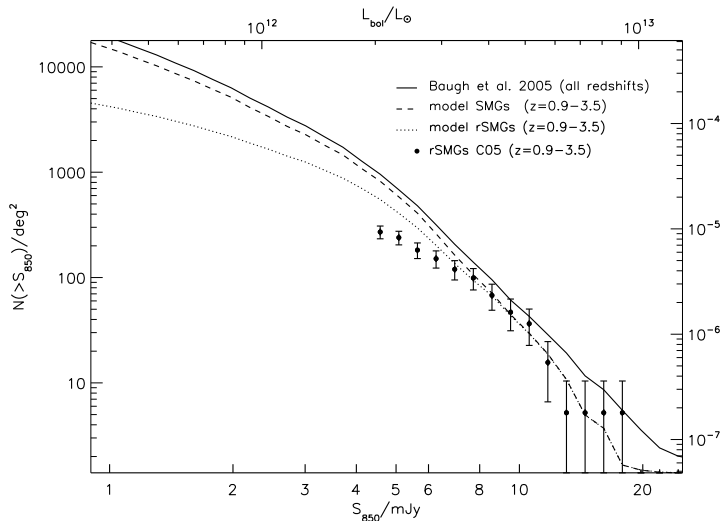


Figure 4. The cumulative number counts per degree² at 850 μ m for galaxies between $z = 0.9$ – 3.5 . The model predictions including all redshifts are shown by the solid line. We also show the expected counts for radio-flux density cuts of $S_{1.4} = 0$ and 30μ Jy, respectively, only considering galaxies in the range $z = 0.9$ – 3.5 . These are compared to the observational counts for SMGs from the C05 redshift survey which are radio selected with $S_{1.4} \gtrsim 30\mu$ Jy, and also in the range $z = 0.9$ – 3.5 . The right-hand axis denotes the approximate space density in physical units, whilst the top axis denotes the approximate bolometric luminosity for galaxies at $z = 2.0$ given their sub-mm flux density.

claimed that the millimeter/sub-millimeter flux density ratio is sensitive to redshift above $z = 3$ (Eales et al. 2003; Greve et al. 2004; Ivison et al. 2005). We therefore compare the far-infrared photometry predicted by the model SMGs and rSMGs with recent observational constraints from Greve et al. (2008) who surveyed the GOODS-North region at 1200 μ m with the Max-Planck bolometer array (MAMBO). For an 850 μ m selected sample, the model galaxies have a median 850/1200 μ m flux density ratio of $S_{850}/S_{1200} = 2.4 \pm 0.2$ between $z = 1.5$ – 3 , and $S_{850}/S_{1200} = 2.2 \pm 0.2$ for a 1200 μ m selected sample with $\sigma_{1200} = 0.7$ mJy over the same redshift range (we note that the error-bars denote the 17 and 84%-ile range, which corresponds to the 1- σ scatter for a Gaussian distribution). Both the 850- and 1200 μ m-selected samples show very little evolution in colour over the redshift range $z = 0.5$ – 5 and are in good agreement with observational constraints (Fig. 5).

3.3.2 350/850 μ m Colours

A better test of the far-infrared properties comes from shorter wavelengths (at $z = 2$ a black-body with a characteristic temperature of $T_d = 35$ K peaks at an observed wavelength of $\sim 300\mu$ m). Prior to the launch of *Herschel*, the most promising route to constrain shorter wavelengths in the far-infrared are 350- and 450 μ m photometry where the atmospheric transmission allows the brightest SMGs to be detected in good conditions.

In Fig. 5 we compare the predicted S_{350}/S_{850} colours with observational constraints. At $z \sim 2$ the median flux density ratio for model SMGs is $S_{350}/S_{850} = 2.5 \pm 2.0$. For comparison, Kovács et al. (2006) and Coppin et al. (2008)

study a total of 27 SMGs at 350 μ m which have secure redshifts. These SMGs have a median flux density ratio $S_{350}/S_{850} = 4.0^{+4.5}_{-2.2}$ (this value includes upper limits for 350 μ m flux densities on three non-detections). Since the data at 350 and 450 μ m suffer from both low number statistics and low signal-to-noise detections we bin the data into two redshift bins, $z < 2$ and $z \geq 2$. As this figure shows, the model predictions seem broadly consistent with the observational data. There is a hint ($< 1.5\sigma$) that the model photometry and data have opposite trends with redshift, but firm conclusions cannot be drawn with the current observational data. However, we stress that this potentially powerful test will be significantly improved with observations of larger samples at higher signal-to-noise from upcoming surveys with SCUBA2 and *Herschel*. In the meantime we note that the model predicts an evolution in the S_{350}/S_{850} flux density ratio for the SMGs and rSMGs is well described by $S_{350}/S_{850} = -0.6 + 11.6 \times (1 + z)^{-1.15}$.

A more useful comparison of the observational and model SEDs can be made by comparing the bolometric luminosities estimated from fits to both real and model photometry. To do this, we fit the 350- and 850 μ m photometry with a modified blackbody of the form $L_\nu \propto B_\nu(T_d)\nu^\beta$ where B_ν is the Planck function evaluated at the emitted frequency ν , and $\beta = 1.5$ (Dunne et al. 2003; Coppin et al. 2008). The result of this fit is a characteristic dust emission temperature T_d for each galaxy, and also an estimate of its bolometric dust luminosity L_{bol} . Kovács et al. (2006) (see also more recently Coppin et al. 2008) demonstrate that sub-mm galaxies have characteristic temperatures consistent with local starbursts ($T \sim 35$ K), but are at least an order of magnitude more luminous in L_{bol} . We can apply the same fitting procedure to the 350- and 850 μ m photometry for all our model SMGs. In this way, we find a median characteristic emission temperature for both model SMGs and rSMGs of $T_d = 32 \pm 5$ K. (Note that simply a characteristic temperature, since GRASIL does not assume a single dust temperature even within a single galaxy.) We also find that the single modified black-body fit (with $\beta = 1.5$) yields an estimated bolometric luminosity which on average is 0.94 ± 0.25 of the true model value (integrated between rest-frame 8 and 1000 μ m). We find that the median bolometric luminosity for model SMGs is $2.0 \pm 1.5 \times 10^{12} M_\odot$. Hence it appears that the far-infrared SEDs of model SMGs are broadly similar to what is inferred from the observations.

With the bolometric luminosities of the model SMGs in hand, we can also investigate how the star-formation rates compare to those inferred observationally. The main difference in the star-formation rates comes from the adoption of the flat IMF in bursts. This results in a much lower star-formation rate per unit bolometric luminosity for SMGs (which are dominated by merger induced bursts). We find that the relation between bolometric luminosity and instantaneous star-formation rate is $\text{SFR}(0.15\text{--}125 M_\odot)(M_\odot \text{ yr}^{-1}) = 1.01 \times 10^{-44} L_{bol}(\text{erg s}^{-1})$ which means that an average model SMG with $L_{bol} = 2 \times 10^{12} L_\odot$ has a star-formation rate of $\text{SFR} = 77 M_\odot \text{ yr}^{-1}$ compared to a typically observationally-derived value of $\text{SFR}(0.1\text{--}100 M_\odot) = 4.5 \times 10^{-44} L_{8\text{--}1000\mu\text{m}}(\text{erg s}^{-1})$ using the Kennicutt (1998) calibration for a Salpeter IMF.

3.4 Radio properties

Although the 1.4GHz radio emission is used to identify the galaxy responsible for the sub-mm emission, the sub-mm/radio flux density ratio has also been used as a diagnostic of both temperature and redshift (Carilli & Yun 1999). However, since the far-infrared colours scale with $(1+z)/T_d$, redshifting a fixed SED template has the same effect as changing the temperature at a fixed redshift, and so without knowledge of the temperature, far-infrared colours cannot be unambiguously used to derive redshifts. Indeed, with a secure redshift for a sub-mm galaxy, the effects of radio identification become apparent: a canonical 5 mJy radio-identified SMG at $z = 2.4$ with a $50\mu\text{Jy}$ radio counterpart has a characteristic dust temperature of 32 K. An increase or decrease in the dust temperature of just 10 K has a dramatic (factor 10 \times) effect on the sub-mm and radio-flux densities and therefore target selection: as the temperature increases for a fixed luminosity, the hotter SEDs mean that the $850\mu\text{m}$ flux density falls below the detection threshold of 5 mJy. Similarly, the coolest SMGs at $z = 2.4$ would have lower radio-flux densities making an SMG undetectable in the radio (Chapman et al. 2004; Blain et al. 2004b, 2003).

In Fig. 5 we compare the predicted $S_{850}/S_{1.4}$ flux density ratio. Both the observations and model galaxies show strong evolution with redshift (a result of strong K-corrections and evolution). The model SMGs have a median flux density ratio $S_{850}/S_{1.4} = 150_{-85}^{+130}$ at $z \sim 2-3$, and so a model SMG with $S_{850} = 5\text{ mJy}$ has $S_{1.4} = 30\mu\text{Jy}$. In the model, the $S_{850}/S_{1.4}$ for model SMGs evolves as $S_{850}/S_{1.4} = -200 + 196 \times (1+z)^{0.53}$.

Whilst the model SMGs appear to reproduce the general evolutionary trend shown by the observations, over the redshift range $z = 0.5-3.5$ they also have a $S_{850}/S_{1.4}$ flux density ratio which is systematically too high compared to the observations, $1.26 \pm 0.24 \times$ (where the error is a bootstrap estimate), despite matching the $z < 0.1$ far-infrared-radio correlation for ULIRGs. For the model rSMGs, we derive $\langle q_L \rangle = 2.19 \pm 0.08$ with $\sigma_{q_L} = 0.20$ – and we find that the radio and submm flux selection do not influence this value. In terms of observations, Kovács et al. (2006) examine the far-infrared-radio correlation for fifteen high redshift SMGs at $z \sim 2$ and derive $\langle q_L \rangle = 2.14 \pm 0.07$ with an intrinsic spread $\sigma_q \sim 0.12$. Compared to ultraluminous far-infrared galaxies at $z = 0$, which have $q_L = 2.34_{-0.10}^{+0.11}$ (see §2.1), we see that the model predicts a similar level of evolution to that seen in the observations. More importantly, the fact that q_L does not change for the model SMGs when we include the observational biases suggests that the low value of q_L found by Kovács et al. (2006) is not a result of sample selection. Instead, it appears that the Kovács et al. (2006) result reflects *real* evolution in the far-infrared-radio correlation. Whether this results from the same starburst age-related evolution found in the model, or from other processes, such as modest contributions to the observed radio flux densities from AGN activity, requires further observational work.

3.5 Restframe UV Properties

With precise positions and redshifts available for the radio-identified SMGs in C05, this sample has also been an impor-

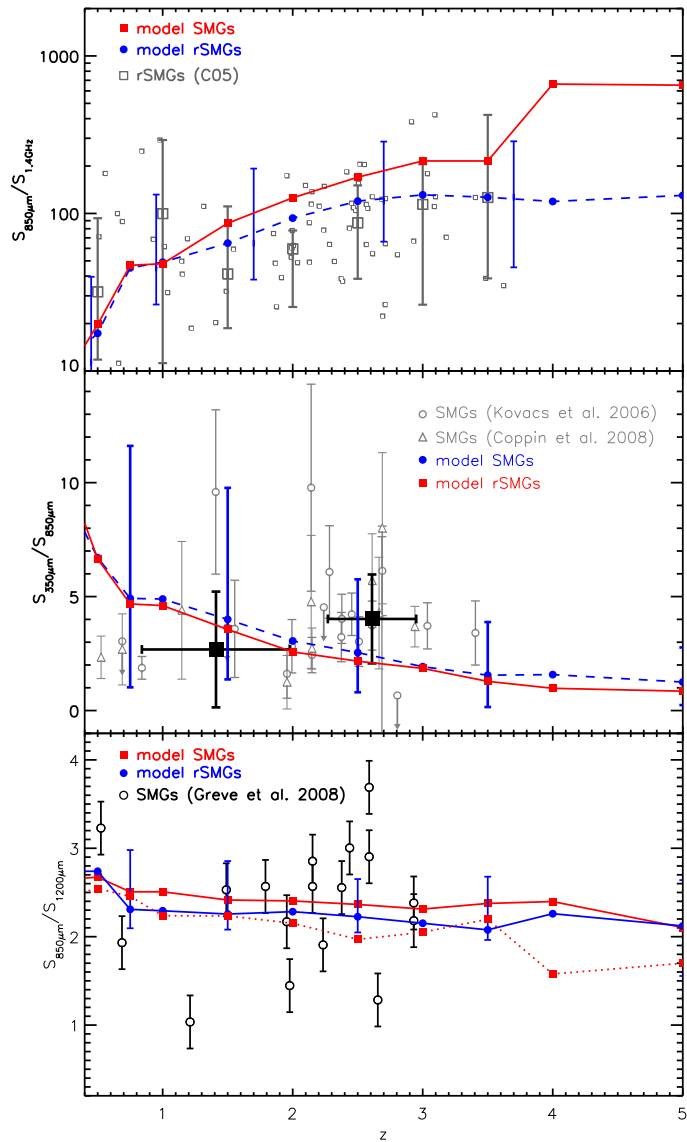


Figure 5. Predicted sub-mm and radio flux density ratios for sub-mm galaxies as a function of redshift. *Top:* $S_{850}/S_{1.4}$ colours of sub-mm galaxies in the C05 sample compared to model SMGs and rSMGs. We plot individual galaxies in the C05 sample and show the median values in redshift intervals of $\Delta z = 0.5$. We also plot the predictions for model SMGs and rSMGs. The error-bars indicate the typical 67%-ile of the model predictions, and, for clarity are shown on alternate points. The model rSMGs have a systematically larger ($\sim 1.26 \pm 0.24 \times$) $S_{850}/S_{1.4}$ flux density ratio than observations suggest over the redshift range $z = 1-4$. *Middle:* S_{350}/S_{850} colours as a function of redshift for model SMGs and rSMGs. The comparison sample is taken from observations at $350\mu\text{m}$ from Kovács et al. (2006) and Coppin et al. (2008) which have good ($> 3\sigma$) detections at $350\mu\text{m}$. Within the observational errors the model SMGs are in good agreement with observations (which suffer from both low number statistics and low-signal to noise detections). To show the redshift trend in the observational data more clearly, we bin the data into two redshift bins ($z < 2$ and $z > 2$) (solid squares). *Bottom:* S_{850}/S_{1200} colours as a function of redshift for model SMGs and rSMGs compared to observations of the GOODS-North regions by Greve et al. (2008). The solid lines denote the evolution for an $850\mu\text{m}$ selected sample, whilst the dotted line represents the evolution for a 2.5 mJy selected sample at $1200\mu\text{m}$ with $\sigma_{1200} = 0.7\text{ mJy}$. Both the model SMGs, rSMGs and $1200\mu\text{m}$ selected model SMGs show remark-

tant basis for more detailed study of the morphologies, stellar populations and stellar/dynamical and halo mass (e.g. Smail et al. 2004; Chapman et al. 2005; Swinbank et al. 2004, 2005, 2006; Borys et al. 2005; Greve et al. 2005; Pope et al. 2006; Tacconi et al. 2006). These studies rely on a combination of high resolution imaging with *HST*, as well as multi-band photometry and spectroscopy from optical, near- and mid-infrared wavelengths. In particular, the stellar populations have been probed using optical, near- and mid-infrared colours to constrain the stellar SED from the rest-frame UV to near-infrared.

The next step in our comparison is therefore to examine the stellar populations and masses of model SMGs. We start by comparing the predicted *B*- and *R*-band magnitudes of SMGs to those from C05. At the median redshift of the C05 sample, the observed *B*- and *R*-bands sample the rest-frame UV, which is very sensitive to the instantaneous SFR, as well as the level of dust extinction. For model SMGs in the redshift range $z = 0.9$ – 3.5 the mean *B*- and *R*-band magnitudes are $B_{AB} = 24.0 \pm 1.3$ and $R_{AB} = 23.9^{+2.0}_{-1.0}$. In comparison the SMGs from C05 have $B_{AB} = 24.8 \pm 1.2$, $R_{AB} = 24.3 \pm 2.0$, slightly fainter and redder than the models predict but with significant overlap (just considering the median (*B* – *R*) colours, we note that an additional obscuration of $E(B - V) = 0.2$ in the model galaxies would make the model *B*–*R* colours agree with observations). The model SMGs have significant overlap in their observed optical colours with BX/BM galaxies: 45% of model SMGs have colours consistent with BX galaxies, whilst another 10% have colours consistent with BM galaxies. This mix of BX/BM is comparable to the observational constraints from C05.

3.6 Restframe Optical Properties

If we turn to longer wavelengths, we can better test the rest-frame optical properties of galaxies predicted by the models against the observations. In Fig. 6 we compare the predicted *K*-band magnitudes of model SMGs with the photometry from Smail et al. (2004). Since the stellar population models do not include emission line components, we have corrected the observed *K*-band photometry for galaxies between $z = 1.8$ – 2.8 (where the strongest optical emission line seen in SMGs, $H\alpha$, falls in *K*) for the $H\alpha$ line emission assuming the median $H\alpha$ equivalent width of $EW_{rest}(H\alpha) = 75 \pm 25 \text{ \AA}$ measured in SMGs (Swinbank et al. 2004). The correction to the *K*-band photometry is $\lesssim 10\%$. In contrast to the optical bands, as Fig. 6 shows, the *K*-band magnitudes of observed SMGs are brighter at a given $850\mu\text{m}$ flux density than all but the brightest model SMGs. However, this plot hides the redshift evolution of the *K*-band magnitude and so a more useful comparison comes from the evolution of *K*-band flux as a function of redshift. As Fig. 6 also shows, at $z \sim 2$ the median observed *K*-band magnitude for SMGs is $K_v = 20.0 \pm 0.3$, which is approximately two magnitudes brighter than the model prediction of $K_v = 22.0 \pm 0.9$ (for both model SMGs and rSMGs).

3.7 Restframe Near-infrared Properties

However, at $z \sim 2$, the observed *K*-band samples the rest-frame *V*-band which is dominated by young stellar popu-

lations. So this comparison is still sensitive to the precise geometry and degree of any dust obscuration – where the models may lack sufficient detail. A more robust test of the predicted photometry from model galaxies comes from a comparison in the rest-frame *K*-band where the effects of dust extinction are much reduced. The rest-frame near-infrared can also provide a better estimate of the mass of the stellar population. At $z \sim 2$, the rest-frame *K*-band is redshifted to $\sim 6\mu\text{m}$, and as such the *Spitzer Space Telescope* has provided unique insight into the stellar masses of far-infrared luminous galaxies.

In particular, Borys et al. (2005) (see also Alexander et al. 2008) estimated rest-frame $2.2\mu\text{m}$ luminosities for a sample of spectroscopically confirmed SMGs in the GOODS-N region from broad-band photometry covering $UBVRIzJK+3.6/4.5/5.8/8\mu\text{m}$ which spans the rest-frame UV, optical and near-infrared at the redshifts of their sample, $z = 0.6$ – 2.9 . They derive $M_K = -26.8 \pm 0.4$ from their sample of ten galaxies at $z > 1.5$. They then estimate a light-to-mass ratio for the stellar population of $L_K/M = 3.2$ using the Starburst99 model (Leitherer et al. 1999) based on an assumed mean age of 200 Myr and a Miller-Scalo IMF (Miller & Scalo 1979) and so infer a typical stellar mass of $\log(M_*) = 2.5^{+3.8}_{-2.5} \times 10^{11} M_\odot$. Borys et al. (2005) estimate that the dust extinction in the rest-frame *K*-band is only $\sim 0.2\text{mag}$ for their galaxies, and so do not correct for it in their stellar mass estimates. In comparison, our model SMGs have median stellar masses $M_* \sim 2.1^{+3.0}_{-1.0} \times 10^{10} M_\odot$, up to an order of magnitude lower than inferred by Borys et al. (2005) (we note that the stellar masses quoted here from both observations and the models include the mass of living stars plus remnants).

However, since deriving the stellar mass is sensitive to the mass-to-light ratio (which depends on the assumed IMF, as well as the age of the stellar population and the dust extinction), a more robust comparison is to simply compare the observed mid-infrared flux densities. In Fig. 7 we compare the predicted $5.8\mu\text{m}$ flux density with observations compiled from deep *Spitzer* surveys (Egami et al. 2004; Hainline 2007; Pope et al. 2006). For $z = 2$ – 3 , observations suggests a median $5.8\mu\text{m}$ flux density of $35 \pm 8 \mu\text{Jy}$. In comparison, the model SMGs have $5.8\mu\text{m}$ flux density of $3.6^{+8.0}_{-2.4} \mu\text{Jy}$, thus under-predicting the $5.8\mu\text{m}$ flux density by a factor $\sim 10\times$. Thus the low rest-frame *K*-band fluxes in the models compared to observations seem to point to the same conclusion about the stellar masses in the model being too low.

We note that the rest-frame stellar mass-to-light ratio for the model SMGs (including dust extinction) is $L_K/M = 4.8 \pm 2.9$. This is not greatly dissimilar to the value used by Borys et al. (2005), but given the different IMFs, stellar ages and dust extinctions assumed, this apparent consistency may be somewhat fortuitous.

This effect of the predicted $5.8\mu\text{m}$ fluxes being lower than observed values is not only limited to the model SMGs. We also use the model to select Lyman-Break Galaxies which have also had extensive mid-infrared follow-up. The median $5.8\mu\text{m}$ flux density of 72 spectroscopically confirmed LBGs between $z = 1.5$ – 3 from Shapley et al. (2005) is $S_{5.8} = 2^{+0.5}_{-1.5} \mu\text{Jy}$ (including non detections). In contrast the median $5.8\mu\text{m}$ flux density for model LBGs selected using the same

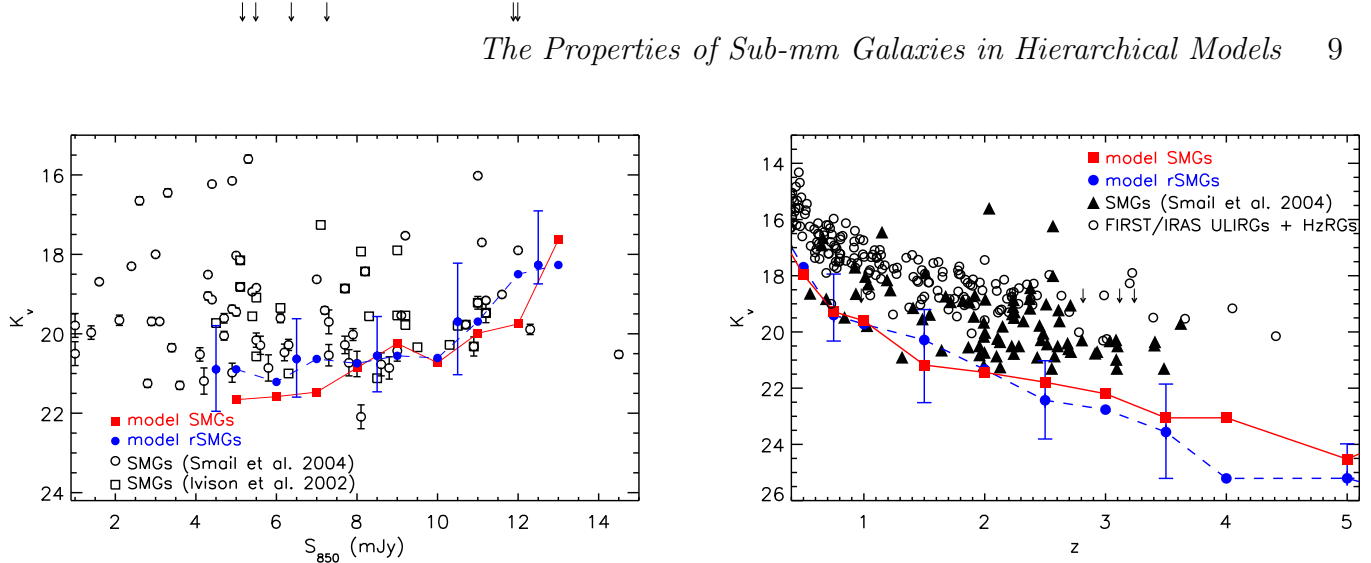


Figure 6. Predicted observed K -band magnitude distribution as a function of redshift and $850\mu\text{m}$ flux density for model SMGs and rSMGs compared to the observations (median values are plotted for the models). The error-bars map the central 67% of the distribution from GRASIL and are shown on alternate points for clarity. Both plots show that the predicted photometry of model SMGs under-estimates that measured from observations by ~ 2 magnitudes ($\sim 6\times$).

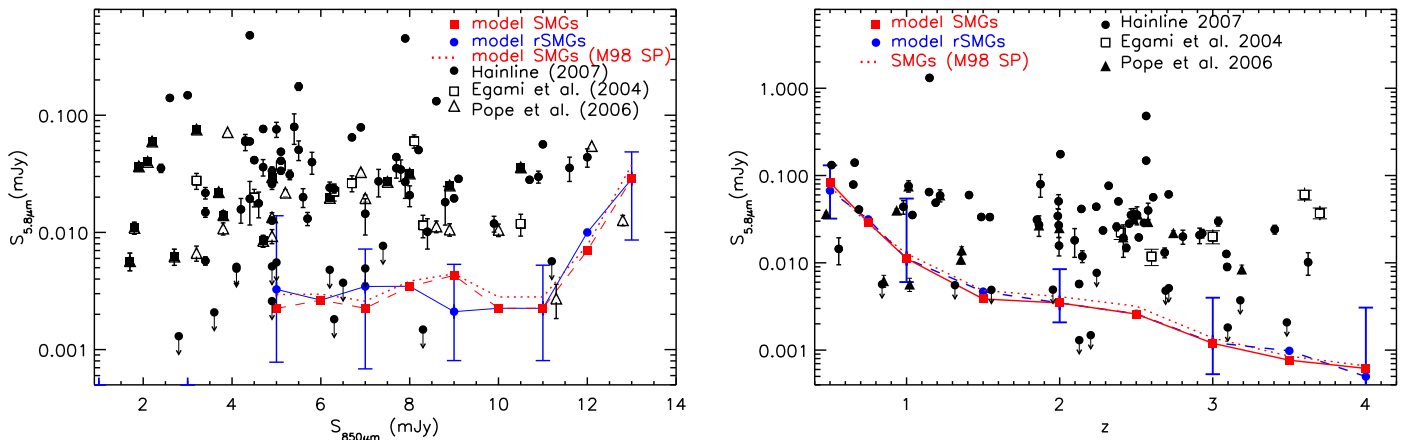


Figure 7. Predictions for the $5.8\mu\text{m}$ flux density of model SMGs as a function of $850\mu\text{m}$ flux density and redshift. In both panels we show the trend of the predicted photometry from GRASIL and the changes which occur when the star-formation histories assume the stellar population synthesis from Maraston (1998) which include a full treatment of TP-AGB stars. The comparison sample comprise SMGs with (secure) spectroscopic redshifts from Hainline (2007); Egami et al. (2004) and Pope et al. (2006). Both plots show that the predicted $5.8\mu\text{m}$ flux density for model SMGs is systematically lower than the observations (by a factor $10\times$), and we suggest that this deficit is due to the lower-than-expected stellar mass for model SMGs ($M_\star \sim 10^{10} M_\odot$ whilst observations suggest more massive systems, $M_\star \sim 10^{11} M_\odot$)

colour cuts and redshift distribution is $S_{5.8} = 0.4^{+0.3}_{-0.2} \mu\text{Jy}$, approximately a factor $4\times$ lower than observations suggest.

Are the low K -band and $5.8\mu\text{m}$ flux densities for model SMGs an effect of the stellar population models rather than an effect of the stellar masses (i.e. is there some way that the models can produce more rest-frame K -band light for the same stellar mass)?

One potential route to reconciling the models with observations is to introduce a full treatment of the thermally-pulsating asymptotic giant branch (TP-AGB) phase into the stellar populations. Recent stellar population synthesis modeling by Maraston et al. (2006) has shown that TP-AGB stars in post-starburst galaxies can contribute significantly to the rest-frame K -band luminosity on $\gtrsim 200$ – 1000 Myr

timescales. Indeed, the predicted stellar light-to-mass ratio at 250 Myr for a single stellar population is $L_K/M \sim 6$ – 8 (Maraston 1998; Maraston et al. 2006). This acts to reduce the observationally estimated stellar mass by a factor of up to $3\times$ if the luminosity weighted stellar populations in the SMGs are dominated by stars with ages of $\gtrsim 200$ – 1000 Myr. However, since sub-mm galaxies are likely to be sustained bursts, the dominant stellar population is likely much younger, and the mass-to-light ratio evolves as a function of the burst age. We note that the median age of a burst in a sub-mm galaxy in the models is 55^{+250}_{-30} Myr (where age denotes the time elapsed since the beginning of the burst). To test the likely effect on the GRASIL luminosities we take the existing star-formation histories and construct the com-

posite stellar population using the Maraston (1998) stellar population models. We use a flat IMF ($x = 0$) in bursts and standard IMF in the quiescent mode, as in our fiducial model. The predicted K -band and $5.8\mu\text{m}$ flux densities are not significantly effected: the observed K -band flux density increases by $\sim 40\%$ at $z = 2$ whilst the $5.8\mu\text{m}$ flux density increases by only $\sim 20\%$ on average (Fig. 7). This suggests a median $5.8\mu\text{m}$ flux density for model SMGs of $\sim 4\mu\text{Jy}$ for the Maraston stellar population models compared to $3\mu\text{Jy}$ for the Padova models at $z = 2-3$, still a factor $8-10\times$ lower than that inferred observationally. Thus, although the TP-AGB phase may have a small effect in the SED modeling, for extended bursts this phase is unlikely to account for the low K -band and $5.8\mu\text{m}$ luminosities predicted for model SMGs.

Another possibility to reconcile the models would be to reduce the burst lifetimes such that the rest-frame near-infrared light becomes dominated by TP-AGB stars. For short bursts (i.e. $< 10\text{Myrs}$), the younger luminosity-weighted age for the stellar population in the SMGs results in a much higher light-to-mass ratio, with $L_K/M = 20-50$ at $15-30\text{Myr}$ (Maraston et al. 2006). However, these shorter bursts are effectively ruled out since the amount of energy required to heat the dust in the sub-mm phase remains fixed, shorter burst durations result in hotter dust temperatures and therefore the $850\mu\text{m}$ sub-mm counts are not matched. This leads us to conclude that the deficit of stellar mass is a real effect and can not be easily explained by either the introduction of the TP-AGB phase into the stellar population models or by dramatically reducing the burst lifetime. We return to this in §5.

One other potential contributor to the low predicted mid-infrared fluxes is the effect of dust extinction in the model. Model SMGs at $z \sim 2$ typically have extinctions of 4 mag in the observed R -band, 2.4 mag in the observed K -band, and 1.6 mag at observer-frame $5.8\mu\text{m}$. This means that the unextincted $5.8\mu\text{m}$ flux would be $4\times$ larger than the extincted value. If the $5.8\mu\text{m}$ dust extinction could be drastically reduced in the model SMGs, while still retaining a large enough extinction in the rest-frame UV to cause most of the UV luminosity to be reprocessed by dust, then this could remove some of the discrepancy between predicted and observed $5.8\mu\text{m}$ fluxes for SMGs, although a significant offset, $\gtrsim 2$, would remain. However, we note that there is support for these high extinctions in the K -band, at least for the emission-line gas. Indeed, studies of the Balmer decrement in SMGs suggest extinctions of order $A_v = 2.9 \pm 0.5$ (Takata et al. 2006). We do not explore this possibility further here, but defer this to a future paper.

Finally, we note that while AGN are ubiquitous in SMGs, their typical contribution to the bolometric emission is $\lesssim 10\%$ (Alexander et al. 2005; Menéndez-Delmestre et al. 2007; Alexander et al. 2008) suggesting that any contamination to the rest-frame $2.2\mu\text{m}$ flux from AGN activity is minimal and unlikely to affect the observed stellar masses. Indeed, as Borys et al. (2005) point out, the shape of the spectral energy distribution is well-described by a stellar model and remove from their analysis the small number of galaxies for which AGN potentially dominate the rest-frame near-infrared.

4 MASSES AND EVOLUTION OF SMGS

4.1 Kinematics and Dynamical Masses

Deriving dynamical masses for high redshift galaxies relies on measuring rotation curves and/or line widths and sizes for the line emitting regions. The most reliable line width estimates for sub-mm galaxies come from resolved dynamics traced through millimetric CO emission (Greve et al. 2005; Tacconi et al. 2006, 2008) and nebular emission (such as H α ; Swinbank et al. 2004, 2006). Converting these line widths into dynamical masses is particularly problematic at high redshift since the sizes of the galaxies are poorly constrained, even with *HST* resolution. We therefore begin by comparing the line widths of the model and observed SMGs. Based on observations of approximately 30 SMGs, $\sigma_{H\alpha} = 170 \pm 30\text{ km s}^{-1}$ and $\sigma_{CO} = 200 \pm 45\text{ km s}^{-1}$ have been derived (Swinbank et al. 2004; Greve et al. 2005; Tacconi et al. 2006, 2008). For the model galaxies the velocity dispersions and sizes are calculated assuming (i) conservation of angular momentum during the collapse of the dark matter halo and baryons; (ii) the size of a stellar spheroid remnant produced by mergers or disk instabilities is determined by virial equilibrium and energy conservation (see Cole et al. 2000 for a detailed discussion). Disks are assumed to have an exponential surface density profile with half mass radius r_{disc} , whilst the spheroid follows an $r^{1/4}$ law in projection with half mass radius (in 3D) r_{bulge} . The mass distribution in the halo and the length scale of the disk and bulge are assumed to adjust adiabatically in response to each other: for the disk the total angular momentum is conserved whilst for the spheroid $rV_c(r)$ is conserved at r_{bulge} . For each galaxy this results in a size and velocity dispersion for the spheroid and a size and rotational velocity for the disk and have been tested against observations by Cole et al. (2000) for local disks and Almeida et al. (2007) for local spheroids.

For both model SMGs and rSMGs we find $\sigma_{1D} = 160 \pm 30\text{ km s}^{-1}$ which is in good agreement with the observational constraints. In order to constrain dynamical masses we also need to include the sizes. However, observationally these are poorly constrained, and usually are taken to be $4-8\text{ kpc}$ (which is approximately the size seen in *HST* observations and in resolved spectroscopic imaging). Using simple dynamical models, observations suggest dynamical masses of order $\sim 2-5 \times 10^{11} M_\odot$ within $4-8\text{ kpc}$ (Swinbank et al. 2006).

Since GALFORM predicts the size and rotational velocity (or velocity dispersion) of the bulge and disk, it is also possible to crudely compare the predicted dynamical masses. In Fig. 8 we show the variation of projected 1-dimensional velocity with spatial scale for sub-mm galaxies which show multiple components in their spatially resolved spectra, either from CO, IFU or longslit observations (Tecza et al. 2004; Swinbank et al. 2004, 2006; Greve et al. 2005; Tacconi et al. 2006, 2008) and overlay the predicted trend of rotational velocity versus size for model SMGs. Although it is clearly difficult to compare the velocity offsets between merging components and the rotational velocity of disks, since the predictions for model SMGs lie within the scatter of the observations, this suggests that the model and observational dynamical masses are in reasonable agreement (moreover, in an ideal system the expected difference between the velocity offset between merging components and

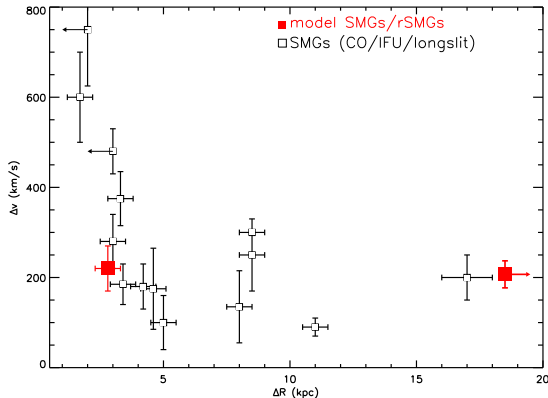


Figure 8. Velocity offset versus spatial offset for the multiple components within sub-mm galaxies from IFU, longslit or CO observations (Tecza et al. 2004; Greve et al. 2005; Swinbank et al. 2004, 2006; Tacconi et al. 2006, 2008). We plot the average radius and velocity of the disk for SMGs and rSMGs from GALFORM showing that the predicted dynamical masses of SMGs are in reasonable agreement with those inferred observationally. We also show the median halo circular velocity and radius for model SMGs ($210 \pm 30 \text{ km s}^{-1}$ and $110 \pm 20 \text{ kpc}$ respectively) at the edge of the plot.

the rotational velocity of a disk is a factor $\sim 2\times$). However, this comparison would benefit from improvements in both the observations and theoretical predictions (e.g. laser guide star adaptive optics integral field spectroscopy would trace the line emitting regions on sub-kpc regions) coupled with a theoretical study of the distribution of detectable emission line gas within dusty, merging systems at high redshift (e.g. from a direct numerical simulation; Okamoto et al. 2005).

4.2 Gas Masses

At its most basic level, the star formation in SMGs is fueled from the reservoirs of cold H_2 gas in these systems. Observations of emission from CO rotational transitions are the primary means of tracing (dipole-less) molecular hydrogen, H_2 . The conversion between CO line luminosity and total cold gas mass is usually expressed via $M_{\text{gas}}/L'_{\text{CO}} = \alpha M_{\odot} (\text{K km s}^{-1} \text{pc}^2)^{-1}$. The standard Milky Way ratio is $M(\text{H}_2+\text{He})/L'_{\text{CO}} = 4.6 M_{\odot} (\text{K km s}^{-1} \text{pc}^2)^{-1}$. However, in the extreme environment near the center of an ultra-luminous galaxy, where the CO emission originates from an inter-cloud medium that is essentially volume filling, rather than from clouds bound by self-gravity, the CO luminosity traces the molecular mass as a whole. Extensive high resolution CO mapping of local ($z < 0.1$) ULIRGs has been used to trace their gas reservoir sizes and dynamics to derive an approximate ratio of $M_{\text{H}_2+\text{He}}/L'_{\text{CO}} \sim 0.8$ (Downes & Solomon 1998; Solomon & Vanden Bout 2005). Adopting this value to convert the CO emission line luminosities of high redshift sub-mm galaxies suggests gas masses $3.0 \pm 1.6 \times 10^{10} M_{\odot}$ within the central 2 kpc (Greve et al. 2005; Tacconi et al. 2006, 2008). Note that if $\alpha > 1$ and assuming random orientations then the H_2 gas mass would exceed the dynamical mass on average.

In the model SMGs, the median gas mass $M_{\text{gas}} = 3.4^{+2.7}_{-1.7} \times 10^{10} M_{\odot}$. A direct comparison of the gas masses

of observed SMGs with those in the models is difficult due to the uncertainty in the conversion between CO(3–2) and CO(1–0) line luminosity as well as the conversion between L'_{CO} and M_{gas} (Hainline et al. 2006). Nevertheless, we can at least test what the value of α would be given the predicted gas masses and observed line luminosities. The median line luminosity of $>5 \text{ mJy}$ SMGs from Greve et al. (2005) and Tacconi et al. (2006) (including non detections) is $L'_{\text{CO}} = 3 \pm 1 \times 10^{10} \text{ K km s}^{-1} \text{ pc}^{-2}$. Assuming the gas mass of model SMGs and rSMGs of $M_{\text{gas}} = 3.4^{+2.7}_{-1.7} \times 10^{10} M_{\odot}$ and using $\alpha = M_{\text{gas}}/L'_{\text{CO}}$ we would require $\alpha = 1.1^{+1.0}_{-0.6} (\text{K km s}^{-1} \text{ pc}^{-2})^{-1}$ to reproduce the observed L'_{CO} , which is in good agreement with the value used to observationally infer gas masses from CO line luminosities in similarly active systems.

4.3 Halo Masses

The clustering of sub-mm galaxies encodes important information on the underlying dark matter distribution (as well as the distribution of SMGs within and between the halos). A measurement of clustering therefore provides key constraints on models of galaxy formation. Although clustering measurements for SMGs are tentative, Blain et al. (2004b) showed the potential of using precise spectroscopic redshifts to detect clustering in modest-sized samples, deriving a crude constraint on their clustering length of $r_0 = 9.8 \pm 3.0 \text{ Mpc}$ (Fig. 9). Using the the Millennium Simulation, Almeida et al. (2008 in prep.) predict that the correlation function of model SMGs from the same model used here is close to a power law of the form $\xi = (r/r_0)^\gamma$ over more than three decades in separation, with $\gamma = -1.94 \pm 0.05$ and a correlation length $r_0 = 8.8 \pm 0.3 \text{ Mpc}$, in excellent agreement with observations.

In Fig. 9 we show the clustering lengths of halos of mass $\log(M_h/M_{\odot}) = 11, 12, 13$ measured from the Millennium Simulation for the evolution of the dark matter in the ΛCDM model (Springel et al. 2005). For a clustering length of $9.8 \pm 3.0 \text{ Mpc}$ the corresponding halo mass is predicted to be $M_h = 3.1^{+5.7}_{-1.9} \times 10^{12} M_{\odot}$ (Gao et al. 2005). This compares to the predicted halo mass for the model SMGs of $M_{\text{halo}} = 3.6^{+5.5}_{-1.5} \times 10^{12} M_{\odot}$. These results confirm the high masses of the SMG host halos in the model. Moreover, the close similarity between the halo masses predicted from their clustering and the actual halo masses of the model SMGs implies that any “merger bias” has only a weak effect on their clustering (Percival et al. 2003).

4.4 Comparison to other galaxy populations

The GALFORM model allows us to compare the SMGs and rSMGs with other high-redshift populations. In this section we briefly discuss the properties of radio unidentified SMGs, as well as optically faint radio galaxies (OFRGs) which have been proposed to have a similar redshift distribution and bolometric luminosities as radio-detected sub-mm galaxies but with comparatively higher dust temperatures (Chapman et al. 2004; Blain et al. 2004a) as opposed to cooler temperatures (or higher redshifts) for the radio undetected SMGs.

To investigate the properties of the model radio undetected SMGs and their relation to the model SMGs, we

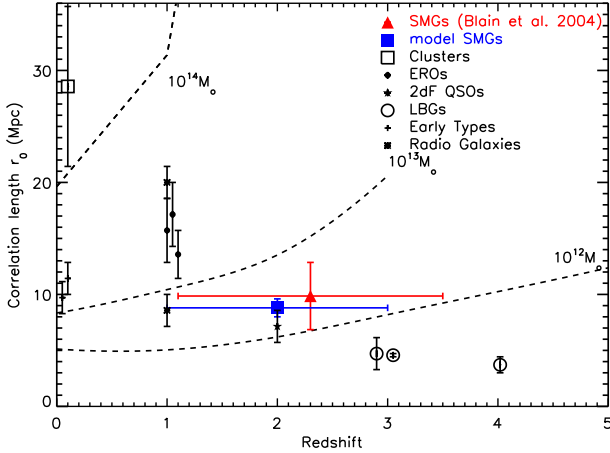


Figure 9. Comoving correlation length for SMGs from Blain et al. (2004b) compared to model SMGs, as well as in contrast to other populations of low- and high-redshift galaxies (Bahcall & Soneira 1983; McCarthy et al. 2001; Croom et al. 2001; Adelberger & Steidel 2000; Willmer et al. 1998; Overzier et al. 2003). The dashed lines show the expected correlation length of dark matter halos as a function of mass and redshift, as measured from the Millennium Simulation (Gao et al. 2005). A clustering length of $r_0 = 9.8 \pm 3.0$ Mpc corresponds to a halo mass of $M_h = 3.1^{+5.7}_{-1.9} \times 10^{12} M_\odot$. This mass is close to that directly predicted for the model SMGs, suggesting that any merger bias is low in our model.

select model galaxies with $S_{850} > 5$ mJy and $S_{1.4} < 30 \mu\text{Jy}$. These have a median redshift of $\langle z \rangle = 2.4$, $\sigma_z = 0.5$, peaking at somewhat higher redshift than the model SMGs ($\langle z \rangle = 2.0$). The bolometric luminosities of the model radio undetected SMGs are comparable to the model SMGs ($L_{bol} = 1.6^{+0.8}_{-1.0} \times 10^{12} L_\odot$), with characteristic dust temperatures slightly colder than model SMGs ($T_d = 28 \pm 8$ K). This supports the suggestion of Chapman et al. (2005) that the radio undetected SMGs are likely to represent the cold wing of the distribution of dust temperatures, but with a similar bolometric luminosity to the radio-detected SMGs. As noted before, this results in a modest bias against the highest redshift SMGs in radio-identified samples.

The halo, stellar and gas masses of this population are $M_{halo} = 2.5^{+7.5}_{-0.8} \times 10^{12}$, $M_\star = 1.5^{+1.7}_{-0.9} \times 10^{10}$ and $M_{gas} = 3.4^{+1.0}_{-1.5} \times 10^{10} M_\odot$ respectively. Thus the properties of the model radio undetected SMGs significantly overlap those of model SMGs, with the main difference arising in their dust temperatures, where the model radio undetected SMGs have marginally colder dust temperatures and similar bolometric luminosities, resulting in a slightly higher redshift distribution compared to model rSMGs.

Similarly, we investigate the properties of the model OFRGs: we define OFRGs as having $S_{850} < 3$ mJy, $S_{1.4} > 30 \mu\text{Jy}$ and $I_{AB} > 22.5$ to be consistent with Chapman et al. (2004). We find that the model OFRGs have a much lower mean redshift than the the model SMGs, with $\langle z \rangle = 1.2$, $\sigma_z = 0.6$. Since these galaxies are selected via their radio flux density, their $850 \mu\text{m}/1.4\text{GHz}$ flux density is lower than the model SMGs with $S_{850}/S_{1.4} = 17^{+5}_{-6}$ at $z = 1$ compared to model SMGs with $S_{850}/S_{1.4} = 50^{+50}_{-30}$ at the same redshift). The halo, stellar and gas masses of OFRGs are $8^{+16}_{-5} \times 10^{11}$,

$4^{+5}_{-3} \times 10^9$ and $1.5^{+0.4}_{-0.5} \times 10^{10} M_\odot$ respectively, and bolometric luminosities of order $6.5 \pm 1.5 \times 10^{11} L_\odot$, approximately $3\text{--}5\times$ lower than the SMGs.

To relate the properties of model SMGs, radio undetected SMGs and OFRGs in Fig 10 we show the predicted $850 \mu\text{m}/1.4\text{GHz}$ flux density ratio as a function of 1.4GHz (rest-frame) radio luminosity, split into four redshift bins ($z \leq 1.5$, $z = 2$, $z = 2.5$ and $z \geq 3$). For comparison we overlay the SMGs from C05. We also show along the top axis the approximate bolometric dust luminosity corresponding to the radio luminosity, computed using the far-infrared-radio correlation defined by the model SMGs (which has the form $\log(L_{bol}/L_\odot) = -14.40 \pm 0.15 + 1.12 \pm 0.02 L_{1.4}$).

As expected, at $z < 1.5\text{--}2$ the model radio-undetected SMGs are cooler with lower bolometric luminosities (lower dust temperatures and lower bolometric luminosities combine to give the same apparent submm flux density as model SMGs). In contrast, at $z > 2.5$ the radio flux density limit cuts into the typical dust temperatures of model SMGs, and so typical model SMGs (which would have been identified at lower redshift) are no longer selected, leaving just the tail of model SMGs with the highest dust temperatures. The observations also show three very low redshift, cold sources (4% of the C05 sample) which are missed in the models. These might arise due to mis-identifications (e.g. 2 radio sources within the beam or an unrelated radio source and a radio undetected SMG within the beam). It is also possible that the model is missing a component of extended cool ULIRG emission (so called cirrus galaxies; e.g. Efstathiou & Rowan-Robinson 2003). We also note that there there are a few high redshift sources with low $S_{850}/S_{1.4}$ flux density ratios and high bolometric luminosities, indicating possible contamination from AGN in some of the higher-redshift sources (or an additional radio component which is not included in the models).

Fig. 10 also shows that the model OFRGs are predicted to have higher dust temperatures than model SMGs, and a range of bolometric luminosities from $L_{bol} \sim 10^{11\text{--}12.5} L_\odot$.

Finally, we also use the model to test what fraction of high-redshift ULIRGs are identified as SMGs. Selecting galaxies with bolometric luminosities comparable to SMGs ($> 2 \times 10^{12} L_\odot$), we find that the model SMGs comprise $\sim 50\%$ and $\sim 40\%$ of the ULIRG population at $z = 1.5\text{--}2.0$ and $z = 2.5\text{--}3.5$ respectively.

4.5 Comparison between the $z \sim 4$ and $z \sim 2$ SMG populations

The negative K-correction experienced at $850 \mu\text{m}$ potentially allows very high redshift (up to $z \sim 8$) galaxies to be detected in the sub-mm (Blain & Longair 1996). The properties of the first sub-mm galaxies ($z \gtrsim 4$) and those at $z \sim 2$ may be very different as the Universe doubles its age over this period. For this reason we have compared and contrasted the predicted properties of the most distant sub-mm galaxies, at $z \gtrsim 4$, with the more typical systems at $z \sim 2$.

In Fig 11 we split the population into two redshift bins ($z = 1\text{--}3$ and $z \geq 3.5$) and compare the halo, stellar and gas mass functions. The model SMGs at $z \geq 3.5$ have typical halo, stellar and gas masses $2.5 \times 10^{12} M_\odot$, $1.0 \times 10^{10} M_\odot$ and $5 \times 10^{10} M_\odot$ respectively. Thus the the $z = 1\text{--}3$ counterparts have halo and stellar masses which are a factor 1.25

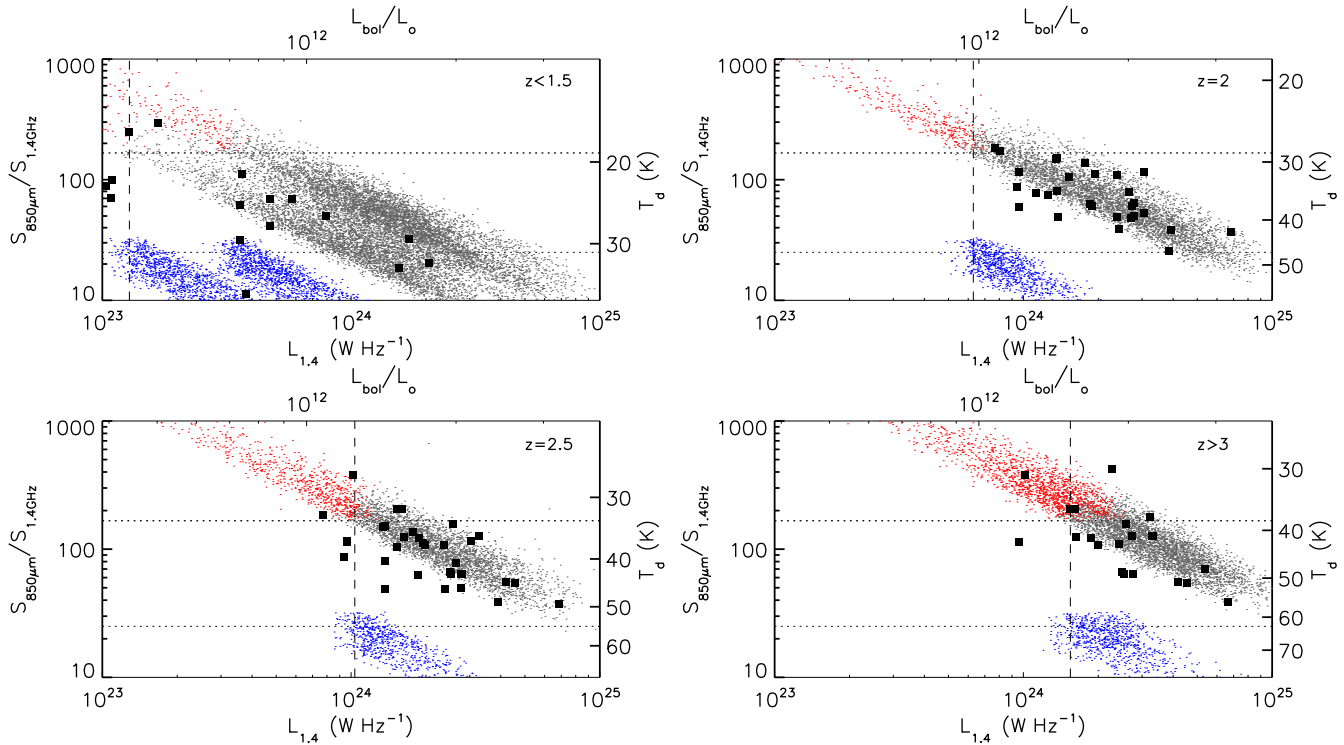


Figure 10. Radio (1.4 GHz) luminosity versus far-infrared/radio flux density ratio as a function of redshift for model SMGs, radio undetected SMGs (ruSMGs) and OFRGs compared to SMGs from Chapman et al. (2005). For clarity we split the data into four redshift bins. We also show the approximate corresponding bolometric luminosity, computed using the far-infrared–radio correlation defined by the model SMGs. We also show the approximate characteristic temperature. The plot shows that at a fixed luminosity, the model radio undetected SMGs have systematically lower temperatures than the model SMGs at each redshift. We also note that (by selection) the model OFRGs have systematically higher temperatures at a fixed luminosity compared to the SMGs at all redshifts.

and $2\times$ larger respectively, with the gas reservoirs a factor $\sim 2\times$ smaller. The bolometric luminosities of the $z = 1-3$ and $z \geq 3.5$ model SMGs are $L_{bol} = 1.8^{+1.5}_{-1.0} \times 10^{12} L_{\odot}$ and $2.8^{+2.2}_{-1.3} \times 10^{12} L_{\odot}$ respectively. Thus the lower redshift model SMGs appear to have slightly lower ($\sim 1.5\times$) bolometric luminosities, although there is significant overlap. This luminosity evolution supports that claimed trend first noted by Ivison et al. (2002) using deep radio and sub-mm imaging. We also note that at $z = 4$ the radio-detected fraction of SMGs is $\sim 30\%$, which is much lower than at $z = 2$ where the radio detected fraction of SMGs is $\sim 95\%$.

Overall, these facts suggest that the $z > 3.5$ model SMGs are physically quite similar to model SMGs at $z = 1-3$. Since there is significant overlap in their properties, the rapid evolution in the redshift distribution and space densities of model SMGs between $z \sim 2$ and $z \sim 4$ seems at first sight puzzling: the negative K-correction means that far-infrared luminous galaxies do not get fainter at $850\mu\text{m}$ as their redshift increases. The explanation of their rapid evolution lies in the hierarchical buildup of structure in the dark matter. The halo masses of model SMGs are similar at both epochs ($> 10^{12} M_{\odot}$), yet the co-moving space density of $> 10^{12} M_{\odot}$ halos at $z \sim 4$ is five times less than at $z \sim 2$. This evolution in the halo number density accounts for most of the change in the number density of model SMGs over this redshift range, although other factors also enter, such as the fraction of halos undergoing major mergers (Lacey & Cole

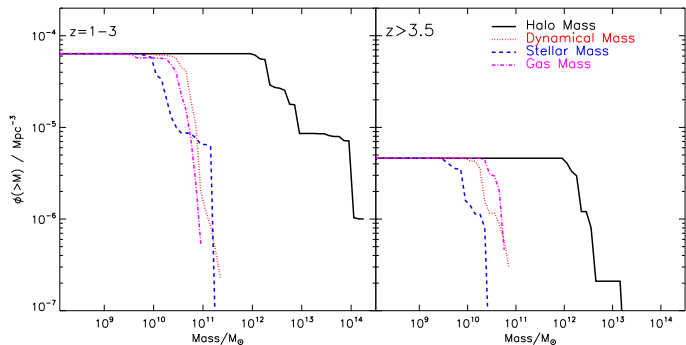


Figure 11. Cumulative mass functions for the halo, dynamical, stellar and gas masses for model SMGs split between at $z \sim 2$ compared to those at $z \sim 4$. The figure shows that the $z \sim 2$ model SMGs are more ubiquitous by a factor $\sim 6\times$ compared to those at $z \sim 4$, but their halo, dynamical, stellar and gas masses are only a factor $\sim 20-40\%$ larger suggesting that the SMG phase occurs in similar types of galaxy at both epochs.

1993), and the fraction of baryons contained in the form of cool gas.

5 DISCUSSION

Our fiducial model has previously been shown to fit the properties of local IRAS galaxies, as well as the number counts of

faint sub-mm galaxies. Here, we have compared the SEDs, dynamical and halo masses of sub-mm galaxies against observational data, showing good agreement with the values measured or inferred from observations. However, the largest discrepancy between the observations and the predictions from the model arises in the observed K -band and mid-infrared photometry. Although we find that in the model SMGs the recent starburst dominates the K -band and mid-infrared flux densities, contributing $\sim 70\%$ at $5.8\mu\text{m}$ and $\sim 80\%$ in the K -band, we find that the K -band fluxes of model SMGs are under-predicted by a factor $\sim 6\times$ compared to observations, whilst the $5.8\mu\text{m}$ fluxes (which corresponds to rest-frame K -band at $z \sim 2$) are under-predicted by a factor $\sim 10\times$. This discrepancy is not limited to the model SMGs, but also applies to other model populations. For example, selecting Lyman-Break Galaxies (using *ugr* colours to select ubiquitous star-forming galaxies at $z \sim 3$) we find that the model LBGs at $z = 2\text{--}3.5$ have $5.8\mu\text{m}$ flux densities a factor $\sim 4\times$ lower than inferred from observations. We show that including a full treatment of the TP-AGB phase in the stellar population modeling (Maraston 1998) cannot make up for this deficit for any plausible star-formation history, since this increases the $5.8\mu\text{m}$ flux densities by only $\sim 20\%$ on average. We also note that within the halo hosting the model SMG, 80–90% of the stellar mass is associated with the model SMG itself, thus including more of the stellar mass from satellites would have little effect on the integrated light.

The low K -band and mid-infrared flux densities are a concern for this model, since this is a key indication of the stellar mass and dust reddening. The obvious interpretation is that the stellar masses of the model SMGs ($M_{\text{star}} \sim 2 \times 10^{10} M_{\odot}$) are too low. However, in the model SMGs the total stellar mass formed in the current burst is $\lesssim 10\%$ of the total stellar mass at the epoch of observation (typically $1\text{--}4 \times 10^9 M_{\odot}$ built in a period of 55_{-30}^{+250} Myr which is the median age of the burst in a model SMG). Furthermore, the total stellar mass formed in all of the previous bursts contributes less than 10% of the total stellar mass of the model SMG at the epoch of observation. This means that the burst mode is responsible for forming less than $\lesssim 20\%$ of the total stellar mass in model SMGs. Since the current burst dominates the luminosity, the rest-frame K -band light-to-mass ratio for the existing- and burst-stellar populations in the model SMGs are very different, with $L_K/M = 1.5_{-0.6}^{+5.0}$ and $L_K/M = 14.5 \pm 9.5$ for the existing- and burst- stellar population respectively. Since the current burst is predicted to dominate the rest-frame K -band luminosity, even though it contains only $\sim 10\%$ of the stellar mass one solution would be to boost the mass in the current burst by a factor ~ 10 . However, if everything else in the model was left unchanged, this would result in an increase in bolometric luminosity by the same factor. However, since the bolometric dust luminosities of SMGs already agree with observations in the current model, this will violate the $850\mu\text{m}$ counts.

Our current model assumes a very flat IMF in bursts, with slope $x = 0$, so one could consider changing this slope. Would steepening the IMF slope to something closer to the Salpeter value $x = 1.35$ (so producing relatively more lower-mass stars), while at the same time increasing the total burst mass, allow the model to increase the K -band luminosity

while keeping the bolometric dust luminosity equal to observed values? To test this we examine the ratio of the K -band-to-bolometric luminosities for both a top-heavy and Salpeter IMF in bursts, but find that this only weakly depends on the IMF slope from $x = 0$ to $x = 1.5$, presumably because both luminosities are dominated by massive stars at these young ages. Thus changing the IMF slope does not seem enough to boost the K -band luminosity by a factor $10\times$ for a fixed bolometric luminosity.

One other potential avenue to increase the predicted near-infrared fluxes in the model SMGs is to alter the dust extinction. As expected, the model SMGs have high dust extinctions, even in the rest-frame K -band, where the extinction is typically about 1.6 mag. Therefore if extinction law could be altered in the model to greatly lower the extinction in the rest-frame K -band, while keeping the extinction high in the rest-frame UV, then the rest-frame K -band luminosities could be boosted by a factor $\sim 4\times$ while keeping the dust bolometric luminosities the same. This would go some way towards resolving the problem with the predicted $5.8\mu\text{m}$ flux densities being too low. However, we note that there is support for these high extinctions in the K -band, at least for the emission-line gas. Indeed, studies of the Balmer decrement in SMGs suggest $A_v = 2.9 \pm 0.5$, thus removing all of the dust extinction in the observed K -band may violate observations constraints. We do not explore this possibility further here, but defer this to a future paper.

Alternatively, is it possible to increase the stellar mass by condensing more gas into stars both prior to and during the sub-mm phase thus boosting the observed K -band and $5.8\mu\text{m}$ luminosities? In order to prevent the over-cooling of baryons into stars (and therefore match the present day K -band luminosity function) the feedback prescription in the B05 model is particularly efficient, with an instantaneous feedback rate, $\beta = \dot{M}_{ej}/\text{SFR} = 1.1\text{--}2.0$ (between $z = 1\text{--}3$) where \dot{M}_{ej} is the gas ejection rate. When recycling from dying stars is included this factor is even more extreme, especially for a top-heavy IMF. In this case, the recycled fraction is $R = 0.9$, thus only 10% of the newly formed stellar mass ends up in long lived stars and remnants (thus the ratio of mass ejection rate to formation rate of long lived stars is $10\text{--}20\times$ during an SMG burst). This efficient feedback results in 55–65% of the baryonic mass in the hot phase for a model SMG at the epoch of observation, with a hot gas mass of $M_{\text{hot}} \sim 8 \times 10^{10} M_{\odot}$ and a total baryonic mass of $M_{\text{bary}} \sim 1.5 \times 10^{11} M_{\odot}$. Thus if the feedback could be reduced, and a substantial fraction of the mass contained within both the cold and hot gas reservoirs could be condensed into stars either prior or during the burst, the result would be an increase in stellar mass of a factor $\sim 6\times$. This has the obvious draw-back that there would be no gas available for future star-formation (unless the halo accretes gas from a merger).

The most promising route to explaining both the near- and far-infrared luminosities in sub-mm galaxies may lie in combining prescriptions in the B05 model with those in Bower et al. (2006) which uses AGN feedback to quench gas cooling in high-mass halos and thus prevent the formation of too many very high-mass galaxies by the present day, rather than relying on very strong supernova feedback, as in the B05 model. In the Bower et al. (2006) model, high-mass galaxies form earlier than in the B05 model, so the stellar

mass function at high redshift has more high-mass galaxies (though both have very similar stellar mass functions at $z = 0$), and this gives better agreement with the observed evolution of the rest-frame K -band luminosity function than for B05. However, the Bower et al. (2006) model in its standard form with a single solar neighborhood IMF under-predicts the sub-mm counts by a factor $\sim 20\times$. We have investigated modifying the Bower et al. (2006) by introducing a top-heavy IMF in bursts, as in the B05 model. We find that we can obtain a comparably good fit to the $850\mu\text{m}$ counts as the B05 model, but the same model then predicts a present-day K -band luminosity function which is too bright by about 1 magnitude at the bright end. However, we have not explored the full parameter space of models combining AGN feedback with a top-heavy IMF, and so it may be that a model can be found which explains both the number counts and rest-frame K -band luminosities of the SMGs, while also being consistent with the observed K -band luminosity function at different redshifts. We will investigate this in more detail in a future paper.

6 CONCLUSIONS

In this paper we have used the GALFORM semi-analytic model for galaxy formation together with the GRASIL spectrophotometric code to investigate in detail the properties of sub-mm galaxies in the model of Baugh et al. (2005). We mimic the observational selection in our model catalogue and identify galaxies both via their $850\mu\text{m}$ and 1.4 GHz (radio) emission. We find that the radio-identified SMGs (rSMGs) are predicted to make up approximately 75% of the whole population. This is in good agreement with the fraction found in observational surveys (eg. Ivison et al. 2005, 2007). The main difference between the radio-identified and radio-unidentified sub-mm galaxies is the characteristic dust temperature, where the radio undetected SMGs are $\sim 10\%$ cooler. This results in model SMGs having a median redshift of $z = 2.0$ whilst model rSMGs (which include a radio flux density threshold $S_{1.4} > 30\mu\text{Jy}$) have a median redshift of $z = 1.7$.

We show that the far-infrared colours of model rSMGs are consistent with observational data. Fitting the 350 and $850\mu\text{m}$ photometry we show that the model far-infrared SEDs are well described by single component modified ($\beta = 1.5$) blackbodies with temperature of $32 \pm 5\text{ K}$ (although GRASIL does not assume a single dust temperature either within or between galaxies). Integrating the model SED and the black-body fit, the inferred and true bolometric luminosities for the model SEDs also agree, with the single modified blackbody fit recovering an average of 0.94 ± 0.25 of the bolometric luminosity. However, the median $850\mu\text{m}/1.4\text{ GHz}$ flux density ratio for SMGs predicted by the model is systematically lower than that observed by a factor $\sim 1.26 \pm 0.24\times$, even after the model has been normalized to match the far-infrared–radio correlation for ULIRGs at $z = 0$. This could be due to evolution in the far-infrared–radio correlation, or due to modest contributions to the observed radio flux density from AGN.

We show that the predicted velocity dispersions are in good agreements with observations, with $\sigma_{1D} \sim 160\text{ km s}^{-1}$ for the model SMGs, compared to observational constraints

of $\sigma = 170\text{--}200\text{ km s}^{-1}$ inferred from the kinematics of the redshifted $\text{H}\alpha$ and CO emission. We also show that the predicted gas masses agree well with those derived from observations using $\alpha = 0.8$. Turning to the halo masses, we find that the model SMGs reside in halos with masses of $M_{\text{halo}} \sim 10^{12.4} M_{\odot}$, and a correlation length of $r_o = 8.8 \pm 0.3\text{ Mpc}$, in excellent agreement with the tentative observational estimate of $r_o = 9.8 \pm 3.0\text{ Mpc}$ from Blain et al. (2004b). We find no evidence for a significant merger bias in the clustering of SMGs in the model.

However, we find that the predicted K -band and mid-infrared ($5.8\mu\text{m}$) flux densities of the model SMGs are up to a factor $10\times$ fainter than observed. We discuss the possible reasons for this. The stellar masses of the model SMGs, $M_{\star} \sim 10^{10} M_{\odot}$, are a factor $10\times$ smaller compared to observational estimates based on the same mid-infrared data ($M_{\star} \gtrsim 10^{11} M_{\odot}$), but the observational estimates are very sensitive to the assumed IMF, burst age and dust extinction. The simplest explanation for this discrepancy in the near- and mid-infrared fluxes is that it is due to the stellar masses being too low in the model. However, other factors may be contributing, for example in the model SMGs, the dust extinction is quite large even at $5.8\mu\text{m}$, resulting in a $4\times$ reduction in the observed flux. If the rest-frame visible and near-infrared dust extinctions in the model SMGs were removed, this would improve (but not eliminate) this discrepancy (an offset of a factor $2\times$ would remain). However, we note that there is support for these high extinctions in the K -band, at least for the emission-line gas. We also discuss possible routes for increasing the near-infrared luminosities and stellar masses, both within the context of the current (Baugh et al. 2005) model, which assumes a top-heavy IMF in bursts, and using the prescriptions described in Bower et al. (2006), which uses AGN feedback to prevent too many baryons cooling in massive halos but assumes a normal IMF throughout. The Bower et al. (2006) model predicts more high-mass galaxies at high redshift, and a K -band luminosity function in better agreement with observations at high redshift, but under-predicts the sub-mm counts by a factor 20. We will discuss the properties of sub-mm galaxies in models which combine features from the Baugh et al. (2005) and Bower et al. (2006) models in a future paper.

We also investigate the evolution of the sub-mm galaxy population in the Baugh et al. (2005) model by comparing the halo and stellar masses for model SMGs at $z = 1\text{--}3$ to those at $z > 3.5$. The $z > 3.5$ SMG population are predicted to make up approximately 2% of the total SMG population (with the $z > 4$ rSMGs contributing approximately 0.5% of the total population). Nevertheless, we find only a mild increase in the halo and stellar masses between $z \sim 4$ and $z \sim 2$, and therefore attribute the strong evolution seen in the redshift distribution primarily to the evolution in the space density of massive halos hosting SMGs.

As well as the need for the models to provide a better match to observations, a number of upcoming surveys and facilities will provide valuable observational constraints which can be used to further test them. In particular, deep SCUBA2 surveys will probe both 450 and $850\mu\text{m}$, providing much tighter constraints on the SEDs of galaxies with bolometric luminosities a factor $10\times$ lower than currently achievable. When combined with results from *Herschel* (which will probe $60\text{--}670\mu\text{m}$), the temperatures, bolometric luminosities

and dust masses of SMGs will be constrained with much higher accuracy than currently possible from the sparse and low signal-to-noise 350 and 850 μm photometry alone. Interestingly, the model predicts that there is a significant tail of faint 450 μm selected galaxies at high redshift (Lacey et al. 2009 in prep). Selecting galaxies with $S_{450} > 2.5$ mJy (the expected 5- σ flux density limit for SCUBA2) the model suggests that there should be ≥ 8000 , 850 and 150 galaxies selected at 450 μm per square degree at $z > 2$, 4 and 5 respectively ($\sim 50\%$, 5% and 1% of the total population respectively), suggesting that the fainter confusion limit at 450 μm may provide the most efficient route to get an unbiased census for the far-infrared selected galaxies at the highest redshifts, providing insights into the physical processes of star-formation occurring at the peak epoch of galaxy formation, $z \sim 2$.

ACKNOWLEDGMENTS

We would like to thank the anonymous referee for providing a number of suggestions which significantly improved the content and clarity of this paper. We thank Claudia Maraston for providing us with stellar population models with a top-heavy IMF, and John Helly and Liang Gao for calculating the merger rates and clustering lengths of halos from the Millennium Simulation. We also gratefully acknowledge Dave Alexander, Richard Bower, Reinhard Genzel and Linda Tacconi for valuable discussions. AMS acknowledges an STFC fellowship. IRS & CMB acknowledge the Royal Society. This work was also supported by the STFC rolling grant for extragalactic astronomy and cosmology at Durham.

REFERENCES

- Adelberger, K. L. & Steidel, C. C. 2000, *ApJ*, 544, 218
 Alexander, D. M., Bauer, F. E., Brandt, W. N., Hornschemeier, A. E., Vignali, C., Garmire, G. P., Schneider, D. P., & Chartas et al. 2003, *AJ*, 125, 383
 Alexander, D. M., Brandt, W. N., Smail, I., Swinbank, A. M., Bauer, F. E., Blain, A. W., Chapman, S. C., & Coppin et al. 2008, *AJ*, 135, 1968
 Alexander, D. M., Smail, I., Bauer, F. E., Chapman, S. C., Blain, A. W., Brandt, W. N., & Ivison, R. J. 2005, *Nature*, 434, 738
 Almeida, C., Baugh, C. M., & Lacey, C. G. 2007, *MNRAS*, 376, 1711
 Bahcall, N. A. & Soneira, R. M. 1983, *ApJ*, 270, 20
 Barger, A. J., Cowie, L. L., Sanders, D. B., Fulton, E., Taniguchi, Y., Sato, Y., Kawara, K., & Okuda, H. 1998, *Nature*, 394, 248
 Baugh, C. M. 2006, *Reports of Progress in Physics*, 69, 3101
 Baugh, C. M., Lacey, C. G., Frenk, C. S., Granato, G. L., Silva, L., Bressan, A., Benson, A. J., & Cole, S. 2005, *MNRAS*, 356, 1191
 Benson, A. J., Bower, R. G., Frenk, C. S., Lacey, C. G., Baugh, C. M., & Cole, S. 2003, *ApJ*, 599, 38
 Benson, A. J., Lacey, C. G., Baugh, C. M., Cole, S., & Frenk, C. S. 2002, *MNRAS*, 333, 156
 Blain, A. W., Barnard, V. E., & Chapman, S. C. 2003, *MNRAS*, 338, 733
 Blain, A. W., Chapman, S. C., Smail, I., & Ivison, R. 2004a, *ApJ*, 611, 52
 —. 2004b, *ApJ*, 611, 725
 Blain, A. W. & Longair, M. S. 1996, *MNRAS*, 279, 847
 Blain, A. W., Smail, I., Ivison, R. J., & Kneib, J.-P. 1999, *MNRAS*, 302, 632
 Borys, C., Smail, I., Chapman, S. C., Blain, A. W., Alexander, D. M., & Ivison, R. J. 2005, *ApJ*, 635, 853
 Bower, R. G., Benson, A. J., Malbon, R., Helly, J. C., Frenk, C. S., Baugh, C. M., Cole, S., & Lacey, C. G. 2006, *MNRAS*, 369, 659
 Bressan, A., Silva, L., & Granato, G. L. 2002, *A&AP*, 392, 377
 Carilli, C. L. & Yun, M. S. 1999, *ApJL*, 513, L13
 Chapman, S. C., Blain, A. W., Ivison, R. J., & Smail, I. R. 2003, *Nature*, 422, 695
 Chapman, S. C., Blain, A. W., Smail, I., & Ivison, R. J. 2005, *ApJ*, 622, 772
 Chapman, S. C., Smail, I., Blain, A. W., & Ivison, R. J. 2004, *ApJ*, 614, 671
 Clements, D. L., Vaccari, M., Babbedge, T., Oliver, S., Rowan-Robinson, M., Davoodi, P., & Ivison et al. 2008, *MNRAS*, 387, 247
 Cole, S., Lacey, C. G., Baugh, C. M., & Frenk, C. S. 2000, *MNRAS*, 319, 168
 Condon, J. J. 1992, *ARAA*, 30, 575
 Coppin, K., Chapin, E. L., Mortier, A. M. J., Scott, S. E., Borys, C., Dunlop, J. S., Halpern, M., & Hughes et al. 2006, *MNRAS*, 372, 1621
 Coppin, K., Halpern, M., Scott, D., Borys, C., Dunlop, J., Dunne, L., Ivison, R., & Wagg et al. 2008, *MNRAS*, 123
 Coppin, K. E. K., Swinbank, A. M., Neri, R., Cox, P., Smail, I., Ellis, R. S., Geach, J. E., & Siana et al. 2007, *ApJ*, 665, 936
 Cowie, L. L., Barger, A. J., & Kneib, J.-P. 2002, *AJ*, 123, 2197
 Croom, S. M., Shanks, T., Boyle, B. J., Smith, R. J., Miller, L., Loaring, N. S., & Hoyle, F. 2001, *MNRAS*, 325, 483
 Downes, D. & Solomon, P. M. 1998, *ApJ*, 507, 615
 Dunne, L., Eales, S. A., & Edmunds, M. G. 2003, *MNRAS*, 341, 589
 Eales, S., Bertoldi, F., Ivison, R., Carilli, C., Dunne, L., & Owen, F. 2003, *MNRAS*, 344, 169
 Efstathiou, A. & Rowan-Robinson, M. 2003, *MNRAS*, 343, 322
 Egami, E., Dole, H., Huang, J.-S., Pérez-Gonzalez, P., Le Floch, E., Papovich, C., & Barmby, P., et al., 2004, *APJS*, 154, 130
 Gao, L., Springel, V., & White, S. D. M. 2005, *MNRAS*, 363, L66
 Genzel, R., Baker, A. J., Tacconi, L. J., Lutz, D., Cox, P., Guilloteau, S., & Omont, A. 2003, *ApJ*, 584, 633
 Granato, G. L., Lacey, C. G., Silva, L., Bressan, A., Baugh, C. M., Cole, S., & Frenk, C. S. 2000, *ApJ*, 542, 710
 Greve, T. R., Bertoldi, F., Smail, I., Neri, R., Chapman, S. C., Blain, A. W., Ivison, R. J., & Genzel et al. 2005, *MNRAS*, 359, 1165
 Greve, T. R., Ivison, R. J., Bertoldi, F., Stevens, J. A., Dunlop, J. S., Lutz, D., & Carilli, C. L. 2004, *MNRAS*, 354, 779

- Greve, T. R., Pope, A., Scott, D., Ivison, R. J., Borys, C., Conselice, C. J., & Bertoldi, F. 2008, ArXiv e-prints, 806
- Hainline, L. J. 2007, Ph.D. Thesis, Caltech Astronomy
- Hainline, L. J., Blain, A. W., Greve, T. R., Chapman, S. C., Smail, I., & Ivison, R. J. 2006, *ApJ*, 650, 614
- Helou, G., Soifer, B. T., & Rowan-Robinson, M. 1985, *ApJL*, 298, L7
- Hughes, D. H., Serjeant, S., Dunlop, J., Rowan-Robinson, M., Blain, A., Mann, R. G., Ivison, R., & Peacock et al. 1998, *Nature*, 394, 241
- Ivison, R. J., Greve, T. R., Dunlop, J. S., Peacock, J. A., Egami, E., Smail, I., & Ibar et al. 2007, *MNRAS*, 380, 199
- Ivison, R. J., Greve, T. R., Smail, I., Dunlop, J. S., Roche, N. D., Scott, S. E., Page, M. J., & Stevens et al. 2002, *MNRAS*, 337, 1
- Ivison, R. J., Smail, I., Barger, A. J., Kneib, J.-P., Blain, A. W., Owen, F. N., Kerr, T. H., & Cowie, L. L. 2000, *MNRAS*, 315, 209
- Ivison, R. J., Smail, I., Dunlop, J. S., Greve, T. R., Swinbank, A. M., Stevens, J. A., Mortier, A. M. J., & Serjeant et al. 2005, *MNRAS*, 364, 1025
- Ivison, R. J., Smail, I., Le Borgne, J.-F., Blain, A. W., Kneib, J.-P., Bezecourt, J., Kerr, T. H., & Davies, J. K. 1998, *MNRAS*, 298, 583
- Kennicutt, R. C. 1998, *ARAA*, 36, 189
- Kovács, A., Chapman, S. C., Dowell, C. D., Blain, A. W., Ivison, R. J., Smail, I., & Phillips, T. G. 2006, *ApJ*, 650, 592
- Lacey, C. & Cole, S. 1993, *MNRAS*, 262, 627
- Lacey, C. G., Baugh, C. M., Frenk, C. S., Silva, L., Granato, G. L., & Bressan, A. 2008, *MNRAS*, 385, 1155
- Leitherer, C., Schaerer, D., Goldader, J. D., Delgado, R. M. G., Robert, C., Kune, D. F., de Mello, D. F., Devost, D., & Heckman, T. M. 1999, *APJS*, 123, 3
- Lilly, S. J., Eales, S. A., Gear, W. K. P., Hammer, F., Le Fèvre, O., Crampton, D., Bond, J. R., & Dunne, L. 1999, *ApJ*, 518, 641
- Maraston, C. 1998, *MNRAS*, 300, 872
- Maraston, C., Daddi, E., Renzini, A., Cimatti, A., Dickinson, M., Papovich, C., Pasquali, A., & Pirzkal, N. 2006, *ApJ*, 652, 85
- McCarthy, P. J., Carlberg, R. G., Chen, H.-W., Marzke, R. O., Firth, A. E., Ellis, R. S., Persson, S. E., & McMahon et al. 2001, *ApJL*, 560, L131
- Menéndez-Delmestre, K., Blain, A. W., Alexander, D. M., Smail, I., Armus, L., Chapman, S. C., Frayer, D. T., Ivison, R. J., & Teplitz, H. I. 2007, *ApJL*, 655, L65
- Miller, G. E. & Scalo, J. M. 1979, *APJS*, 41, 513
- Okamoto, T., Eke, V. R., Frenk, C. S., & Jenkins, A. 2005, *MNRAS*, 363, 1299
- Overzier, R. A., Röttgering, H. J. A., Rengelink, R. B., & Wilman, R. J. 2003, *A&AP*, 405, 53
- Percival, W. J., Scott, D., Peacock, J. A., & Dunlop, J. S. 2003, *MNRAS*, 338, L31
- Pope, A., Scott, D., Dickinson, M., Chary, R.-R., Morrison, G., Borys, C., Sajina, A., & Alexander, D. et al. 2006, *MNRAS*, 370, 1185
- Salpeter, E. E. 1955, *ApJ*, 121, 161
- Sanders, D. B., Mazzarella, J. M., Kim, D.-C., Surace, J. A., & Soifer, B. T. 2003, *AJ*, 126, 1607
- Scott, S. E., Fox, M. J., Dunlop, J. S., Serjeant, S., Peacock, J. A., Ivison, R. J., Oliver, S., & Mann, R. et al. 2002, *MNRAS*, 331, 817
- Shapley, A. E., Steidel, C. C., Erb, D. K., Reddy, N. A., Adelberger, K. L., Pettini, M., Barmby, P., & Huang, J. 2005, *ApJ*, 626, 698
- Silva, L., Granato, G. L., Bressan, A., & Danese, L. 1998, *ApJ*, 509, 103
- Smail, I., Chapman, S. C., Blain, A. W., & Ivison, R. J. 2004, *ApJ*, 616, 71
- Smail, I., Ivison, R. J., & Blain, A. W. 1997, *ApJL*, 490, L5
- Smail, I., Ivison, R. J., Blain, A. W., & Kneib, J.-P. 2002, *MNRAS*, 331, 495
- Smail, I., Ivison, R. J., Owen, F. N., Blain, A. W., & Kneib, J.-P. 2000, *ApJ*, 528, 612
- Solomon, P. M. & Vanden Bout, P. A. 2005, *ARAA*, 43, 677
- Springel, V., White, S. D. M., Jenkins, A., Frenk, C. S., Yoshida, N., Gao, L., Navarro, J., & Thacker et al. 2005, *Nature*, 435, 629
- Swinbank, A. M., Chapman, S. C., Smail, I., Lindner, C., Borys, C., Blain, A. W., Ivison, R. J., & Lewis, G. F. 2006, *MNRAS*, 371, 465
- Swinbank, A. M., Smail, I., Bower, R. G., Borys, C., Chapman, S. C., Blain, A. W., Ivison, R. J., & Howat, S. R. et al. 2005, *MNRAS*, 359, 401
- Swinbank, A. M., Smail, I., Chapman, S. C., Blain, A. W., Ivison, R. J., & Keel, W. C. 2004, *ApJ*, 617, 64
- Tacconi, L. J., Genzel, R., Smail, I., Neri, R., Chapman, S. C., Ivison, R. J., Blain, A., & Cox et al. 2008, ArXiv e-prints, 801
- Tacconi, L. J., Neri, R., Chapman, S. C., Genzel, R., Smail, I., Ivison, R. J., Bertoldi, F., & Blain et al. 2006, *ApJ*, 640, 228
- Takata, T., Sekiguchi, K., Smail, I., Chapman, S. C., Geach, J. E., Swinbank, A. M., Blain, A., & Ivison, R. J. 2006, *ApJ*, 651, 713
- Tecza, M., Baker, A. J., Davies, R. I., Genzel, R., Lehnert, M. D., Eisenhauer, F., Lutz, D., & Nesvadba et al. 2004, *ApJL*, 605, L109
- Vlahakis, C., Eales, S., & Dunne, L. 2007, *MNRAS*, 379, 1042
- Webb, T. M. A., Lilly, S. J., Clements, D. L., Eales, S., Yun, M., Brodwin, M., Dunne, L., & Gear, W. K. 2003, *ApJ*, 597, 680
- Willmer, C. N. A., da Costa, L. N., & Pellegrini, P. S. 1998, *AJ*, 115, 869
- Younger, J. D., Fazio, G. G., Huang, J.-S., Yun, M. S., Wilson, G. W., Ashby, M. L. N., Gurwell, M. A., & Lai et al. 2007, *ApJ*, 671, 1531
- Yun, M. S., Reddy, N. A., & Condon, J. J. 2001, *ApJ*, 554, 803

This paper has been typeset from a \TeX / \LaTeX file prepared by the author.